5-2021

Design and Modeling a Tunable Non-Hermitian Acoustic Filter

Sandeep Puri
The University of Texas Rio Grande Valley

DESIGN AND MODELING A TUNABLE NON-HERMITIAN ACOUSTIC FILTER

A Thesis

by

SANDEEP PURI

Submitted to the Graduate College of
The University of Texas Rio Grande Valley
In partial fulfillment of the requirements for the degree of

MASTER OF SCIENCE

May 2021

Major Subject: Physics

DESIGN AND MODELING A TUNABLE NON-HERMITIAN ACOUSTIC FILTER

A Thesis
by
SANDEEP PURI

COMMITTEE MEMBERS

Dr. Hamidreza Ramezani
Chair of Committee

Dr. Nicholas Dimakis
Committee Member

Dr. Volker Quetschke
Committee Member

May 2021

ABSTRACT

Puri, Sandeep., Design and Modeling of a Tunable non-Hermitian Acoustic Filter. Master of Science (MS). May 2021, 65 pp, 2 tables, 32 figures, references, 62 titles.

In this thesis, we explore an application of a non-Hermitian acoustic system with tunable loss in filtering specific frequencies from an upcoming signal at will. Using the commercial computational software, we design our proposed tunable filter made of a phononic super-lattice. The super-lattice consists of two sublattices connected in series. The first sublattice is Hermitian, whereas the other can be Hermitian or Non-Hermitian depending on the amount of loss induced in it. By introducing the loss in the system, we observe the generation of absorbed resonances that can be seen in the reflection spectrum. The range of the filtered frequencies can be controlled by adjusting the degree of non-Hermiticity and designing the first sublattice's resonances. The resonances in the first sub-lattice can be adjusted by increasing or decreasing the number of unit cells in the sub-lattice. Our tunable acoustic filter can be extended to higher frequency ranges, such as ultrasound and other areas, such as photonics. In addition, we explore the geometry-induced non-Hermitian mode couplings and study the different modes in a system of acoustic ring resonators with induced loss and study the field localization within the system.

DEDICATION

To My Parents

ACKNOWLEDGEMENTS

First of all, I would like to thank my advisor Dr. Hamidreza Ramezani, for his immense care and support throughout my time here at the UTRGV. He's been an important part of my professional growth since I've met him. He is more like an elder brother than an advisor to me.

I would like to express my sincere gratitude to my other committee members Dr. Nicholas Dimakis and Dr. Volker Quetschke for their assistance in my education. I extend my heartfelt gratitude to the faculty of the Department of Physics and Astronomy, especially Dr. Soma Mukherjee and Dr. Ahmed Touhami for helping me with my Ph.D. application.

I acknowledge the University of Texas Rio Grande Valley and the Department of Physics and Astronomy for the financial support and for providing me the opportunity to study and research.

My special thanks to my friends and labmates Jannatul Ferdous (Rima) and Guilei Zhu for being wonderful colleagues and for their valuable suggestions.

I am indebted to my family. I am always thankful to my parents for all the sacrifices they have made for me. I want to thank my siblings, my elder brother for always supporting me in my life decisions, and my younger sister for being there to support me. My fiancé for her support and being a wonderful partner.

Lastly, I would like to thank everybody for their every little contribution to making me who I am.

TABLE OF CONTENTS

Page

LIST OF TABLES

Page

LIST OF FIGURES

Page

CHAPTER I

INTRODUCTION

1.1 Background

Being able to control the propagation of sounds and phonons at will is the long-desired goal of modern physics and applications. The latest development of metamaterials has made remarkable achievements in acoustics and phonon transport manipulation. Recently, phononic crystals have become a subject of importance for many potential applications, due to the existence of a complete bandgap in its band structure. The phononic crystals find their application in numerous fields including vibration isolation, noise suppression, sound barriers, filters, waveguides, and transducers to name a few (Aly & Mehaney, 2012; Chen et al., 2008; Pennec et al., 2010; Xiao et al., 2013). However, the practical frequency and bandgaps tunability of phononic crystals are the key challenges in order to make them into actual devices in various technical fields (Bergamini et al., 2014; Robillard et al., 2009). Many attempts have been made to achieve tunability, such as thermal tuning(Bian et al., 2014), electromechanical tuning(Celli & Gonella, 2015), piezoelectric shunting (Hou & Assouar, 2015), external magnetic fields (Allein et al., 2016; Bilal et al., 2017; Robillard et al., 2009; Vasseur et al., 2011), static loads (P. Wang et al., 2014), embedded electromagnets (Z. Wang et al., 2016), nonlinear effects (Boechler et al., 2011; F. Li et al., 2014; Liang et al., 2010), and acoustic trapping (Caleap & Drinkwater, 2014). All these works are focused on the lattice geometry, density, and sound velocity contrast, which are the main parameters that affect the frequency and width of the bandgap.

Recently, a new perspective has emerged that incorporates non-Hermiticity to propose new physics and manipulate sound propagation in acoustic media (Fleury et al., 2015; Zhu et al., 2014). The degree of non-Hermiticity is induced through the loss and gain mechanism embedded in the phononic structure, by means of effective complex bulk modulus and mass density. Although many types of research have been conducted on the effect of losses on the propagation of sound waves (Andreassen & Jensen, 2013; Jensen, 2003; Langley, 1994; Molerón et al., 2016; Morse & Ingard, 1986), their occurrence has been ignored due to their well-known negative effects on the performance of the acoustic materials studied (Ward et al., 2015). Recently fascinating and peculiar achievements obtained in the non-Hermitian system and judiciously introduced balanced absorption (Feng et al., 2017) and amplification mechanisms has inspired new ideas to incorporate the degree of non-Hermiticity in the acoustic systems. Several noticeable theoretical and experimental parity-time symmetric acoustic structures have been proposed so far (Aurégan & Pagneux, 2017; Christensen et al., 2016; Ding et al., 2015; Y. Li et al., 2017; Poshakinskiy et al., 2016; Ramezani et al., 2016; Shi et al., 2016; Zhang et al., 2015), however, practical application of PT non-Hermitian acoustic structures is still missing.

The main objective of this study is to design a tunable acoustic filter with the help of induced non-Hermiticity in the system. The non-Hermiticity is induced as losses in a phononic lattice. The loss in the system can be changed in order to alter the degree of non-Hermiticity. Based on which we can filter/eliminate specific frequencies from an upcoming signal at will. Using commercial computational software, we design our proposed tunable filter made of a phononic super-lattice. The working principle and its details will be discussed in more detail further in later chapters.

1.2 Thesis Organization

The central theme of this thesis is to design and characterize an acoustic filter based on the application of a non-Hermitian acoustic system. This thesis consists of four chapters. The purpose of the present chapter is to briefly introduce the purpose and motivation of this thesis. The other three chapters are organized in the following manner:

In Chapter 2, We will briefly introduce phononic crystals. We will discuss its basic properties and its band structure, the parameters that affect the bandgap of the phononic lattice, and how to use non-Hermiticity to tune its bandgap. We will conclude by introducing some applications of phononic crystals as acoustic filters.

In Chapter 3, We will briefly discuss the simulation steps and techniques that we used to simulate our proposed model.

In Chapter 4, We will introduce our proposed model. Discuss the results obtained from the simulation. Design the realistic model and show that the induced loss in the model can be created by designing the side holes in one of the two sublattices of the phononic superlattice. Compare the simulation results of the proposed model and the realistic model. Finally, we will summarize the tunable acoustic filter we proposed and designed and its working principle.

In Chapter 5, We study the geometry-induced non-Hermitian mode couplings and study the different modes in a system of non-Hermitian acoustic ring resonators. We study the field localization within the system.

In Chapter 6, We will conclude with a review of the key points and future prospects of the project.

CHAPTER II

PHONONIC CRYSTALS AND NON-HERMITIAN ACOUSTIC SYSTEM

2.1 Introduction

Phononic crystals (PnCs) are a type of synthetic periodic material that is used to control and manipulate the propagation of elastic (or acoustic waves). In other words, we can say the phononic crystals (PnCs) are the acoustic or elastic analog of the photonic crystals for electromagnetic waves (Khelif & Adibi, 2016). The periodic nature of PnC gives them novel properties that cannot be found in bulk materials. For example, PnC can exhibit phononic band gaps, which are frequency ranges in which sound waves are prohibited from propagating inside PnC. It composes of the periodic structure of different acoustic velocities and densities with lattice constants on the scale of the wavelength of the sound (or ultrasound). Adding defects to an ideal PnC with a phononic bandgap, devices such as waveguides and cavities can be designed to control the propagation of sound waves in the bandgap and achieve novel functions in a very compact structure. The first phononic bandstructure for two-dimensional lattices of solid cylinders in the solid background was calculated simultaneously by Sigalas(M. Sigalas & Economou, 1993) and Economou and Kushwaha et al (M. S. Kushwaha et al., 1993).

The first experimental measurement of sound attenuation due to periodicity was carried out under atmospheric conditions by E. Sempere on a sculpture, which was displayed in the open air

of Madrid (Fig. 2.1). In 1998, the first phononic crystals with a complete bandgap were reported for the periodic structure of a square lattice of cylindrical holes filled with mercury and drilled in an aluminum alloy plate (Sánchez-Pérez et al., 1998) (Montero de Espinosa et al., 1998). In the past few years, various periodic structures with phononic band gaps in various frequency ranges have been fabricated.

In this chapter, we will review the properties of the phononic crystals and the concept of the bandstructure. The occurrence of the band gaps in its band structures and its dependence on the physical and geometrical parameters with the examples of different types of phononic crystals. We will give explore the effects of non-Hermiticity on the band structure and the propagation of waves in the phononic crystals and conclude with some applications.

2.2 Fundamental Properties of Phononic Crystals and their Band Structures

Controlling and manipulating acoustic/elastic waves is a fundamental problem with a wide range of applications, especially in the field of information and communication technologies. The propagation of the wave in a periodic medium is based on the dynamical equations of motion. The propagating sound wave oscillates with time and is consistent with the coordinate sequence of the material displacement, and is accompanied by similar pressure and/or shear elastic stress patterns. For a homogeneous and isotropic elastic medium characterized by mass density, ρ, speed of longitudinal, c_l, and transverse, c_t sound, the derivation of the wave equation can be found (Olsson III & El-Kady, 2009). The longitudinal and transverse sound waves decouple and propagate independently in a homogeneous bulk medium, t. The displacement vector field **u** is potential in a longitudinal wave ($\nabla \times \mathbf{u} = 0$) and it is solenoidal ($\nabla . \mathbf{u} = 0$) in a transverse wave. The requirement of continuity of the displacements and stresses

Fig. 2.1 E. Sempere's sculpture in Madrid shows a two-dimensional phononic crystal composed of steel rods with a diameter of 2.9 cm arranged in a square lattice with a period of 10 cm (Deymier, 2013).

leads to the mixing of these two modes in presence of a boundary. From the theory of surface Rayleigh waves (Landau et al., 1986), it is known that the total elastic displacement is a superposition of potential and solenoidal fields and thus cannot be decoupled. Similarly, the longitudinal and transverse displacements also cannot be split in the general case of an arbitrary inhomogeneous elastic medium. The equation of motion for the components of the displacement

vector contains both velocities, c_l, and c_t, (M. S. Kushwaha et al., 1993; M. Sigalas & Economou, 1993) and can be written as follows:

$$\rho \frac{\partial^2 u_i}{\partial t^2} = \nabla.(\rho c_t^2 \nabla u_i) + \nabla.\left(\rho c_t^2 \frac{\partial \boldsymbol{u}}{\partial x_i}\right) + \frac{\partial}{\partial x_i}[(\rho c_t^2 - 2\rho c_t^2)\nabla.\mathbf{u}] \quad (2.1)$$

Here $\rho = \rho(\boldsymbol{r})$, $c_l = c_l(\boldsymbol{r})$, and $c_t = c_t(\boldsymbol{r})$ are arbitrary functions of radius-vector $\boldsymbol{r} = (x_1, x_2, x_3)$.

In phononic crystals, all functions that characterize material properties are periodic in space and can be explained in the Fourier series of the infinite reciprocal lattice vector **G**;

$$\rho(r) = \Sigma_G \, \rho(G) \exp(i\boldsymbol{G}.\boldsymbol{r}), \quad (2.2)$$

Where the Fourier component is defined as follows:

$$\rho(\boldsymbol{G}) = \frac{1}{V_c} \int_{V_c} \rho(\boldsymbol{r}) \exp(i\boldsymbol{G}.\boldsymbol{r}) \, d\boldsymbol{r}, \quad (2.3)$$

Here the integral is taken over the volume of the unit cell V_c, and in the case of 2D periodicity, it is replaced by the area of the unit cell A_c, or by the lattice period l_c for 1D superlattices. The displacement vector **u** is the solution of the wave equation (2.1), which satisfies the Bloch theorem and can be expanded on the reciprocal lattice vector

$$\mathbf{u}(\mathbf{r}) = \mathbf{u}_k(\boldsymbol{r}) = \exp(i\boldsymbol{k}.\boldsymbol{r}) \, \Sigma_G \mathbf{u}_k(\boldsymbol{G}) \exp(i\boldsymbol{G}.\boldsymbol{r}). \quad (2.4)$$

The Bloch vector **k** plays the role of the phononic momentum and its possible values scan the interior of the irreducible part of the Brillouin zone. Substituting the Fourier expansions (2.2) and (2.3) we obtain a set of linear homogeneous equations for the coefficients $\mathbf{u_k}(\mathbf{G})$. If the determinant of the set of equations disappears, then the set has a non-trivial solution. Generally, this condition defines the dispersion relation which gives the infinite number of allowable

frequencies $\omega_n(\mathbf{k})$, (n = 1, 2, 3, …) corresponding to the frequency bandstructure of each value of the Bloch vector **k**. In practice, the size of the determinant and the number of allowed frequencies (bands) are limited by the finite number of plane waves (reciprocal lattice vectors) in the expansions (2.2) and (2.4). This method of calculating the phonon band structure, namely "plane wave extension", is the most popular one. There are numerous examples of phononic bandstructure calculation with this method (M. S. Kushwaha et al., 1993; Manvir S. Kushwaha, 1997; Montero de Espinosa et al., 1998; Vasseur et al., 2001).

2.2.1 Quasi-Static Limit and the Method of PlaneWaves

We know that the scattering cross-section decreases with decreasing frequency, which means that waves propagating through an inhomogeneous medium at a sufficiently low frequency will be subject to very weak multiple scattering. Therefore, in the first approximation, it is a plane wave. According to this conclusion, the main contribution to the Fourier expansion Eq.(2.4) comes from the term with **G** = 0 and all the other terms with **G**≠0 vanish linearly at $\omega \to 0$. Using this property one can calculate the effective speed of the sound as

$$c_{eff} = \lim_{k \to 0} \frac{\omega}{k}. \tag{2.5}$$

The effective frequency region of this formula is consistent with the linear dispersion interval $\omega = c_{eff}k$ in the lowest allowable frequency band. Here, not only the wavelength of 2π/k but also the wavelength of each component exceeds the size of the unit cell. Under these conditions, all the structural details of the photonic crystal cannot be resolved by sound waves. However, this does not mean the effective sound velocity Eq. (2.5) is only determined by the average parameters of the structure. The exact formula for the effective sound velocity includes the contribution of all reciprocal lattice vectors **G**.

The value of c_{eff} obtained from equation (2.5) corresponds to the quasi-static limit. Within this limit, the effective medium does not exhibit internal resonance, and the dispersion relationship is linear. Limited but still lower frequencies, internal resonances may appear in the scattering cross-section.

2.2.2 One-Dimensional Periodicity

When the dispersion relationship can be obtained in a closed form, the case of one-dimensional phononic crystals, the so-called superlattices, is an important special case. A superlattice is a periodic sequence of two (or more) layers of various elastic materials arranged in a regular pattern. We mark the characteristics of each material by sub-index a and b. In this special case, if the Bloch vector **k** is oriented along the superlattice axis (z-axis), the waves with longitudinal and lateral polarization will propagate independently. For example, considering a longitudinal wave with $u_z \sim \exp(ikz - i\omega t)$, the following dispersion equation can be obtained by directly matching the boundary conditions at the interface and applying Bloch's theorem (Farnell, 1988) (Bloch, 1929).

$$\cos kd = \cos\left(\frac{\omega a}{c_a}\right)\cos\left(\frac{\omega b}{c_b}\right) - \frac{1}{2}\left(\frac{z_a}{z_b} + \frac{z_b}{z_a}\right)\sin\left(\frac{\omega a}{c_a}\right)\sin\left(\frac{\omega b}{c_b}\right). \quad (2.6)$$

Here $d = a + b$ is the period of the superlattice, where the unit cell contains two layers with widths a and b. The elastic material of the layer is characterized by the velocities of longitudinal sound c_a and c_b and acoustic impedances $z_a = \rho_a c_a$ and $z_b = \rho_b c_b$. For pure transverse waves, the form of the dispersion equation is the same as eq. (2.6), where c_a and c_b are the speed of transverse sound waves (Camley et al., 1983).

For each value of the Bloch vector k lying within the Brillouin zone, $|k| \leq \pi/d$ Eq. (2.6) determines the infinite number of frequencies forming the band structure $\omega = \omega(k)$. We can see

that within a certain frequency interval, the absolute value of the expression in the RHS of Eq. (2.6) may exceed one. In fact, for any arbitrarily small value of the acoustic contrast between impedances, the sum $(z_a/z_b + z_b/z_a)/2$ exceeds one, so this is also true for the RHS as a whole. The frequency interval where the RHS exceeds one in formula (2.6) corresponds to the phononic bandgap. Sound waves with frequencies in any gap will not propagate.

In the quasi-static limit when $kd, \omega\, a/c_a, \omega b/c_a \ll 1$, the trigonometric functions in Eq. (2.6) can be expanded. Keeping quadratic over ω and *k* terms the following linear relation is obtained:

$$\omega = c_{eff} k. \tag{2.7}$$

Linear dispersion indicates that the superlattice behaves like a homogeneous elastic medium with the speed of sound c_{eff}. The elastic parameters of the effective homogeneous medium are given by the following relations

$$\frac{1}{B_{eff}} = \frac{\beta}{B_a} + \frac{1-\beta}{B_b}, \rho_{eff} = \beta\rho_a + (1-\beta)\rho_b, c_{eff} = \sqrt{\frac{B_{eff}}{\rho_{eff}}}\,. \tag{2.8}$$

Here, $\beta = a/d$ is the filling fraction of the component a. The effective bulk constant and effective mass density are both positive and consistent with their static values. Dynamic effects may lead to negative values of ρ_{eff} in the vicinity of internal resonance. In a one-dimensional phononic crystal, local resonances appear if the unit cell consists of three or more layers of different elastic materials (Grimsditch, 1985; Nemat-Nasser et al., 2011).

2.3 Dispersion Curves and Band Gaps in Phononic Crystals:

The concept of phononic crystal was followed by the similar concept of photonic crystals which are used to propagate electromagnetic waves (Joannopoulos, 2008; Yablonovitch, 1987). The phononic crystals were introduced especially looking for the possibilities of absolute band-

gap (Pennec et al., 2010; Mihail Sigalas et al., 2005). Similar to the photonic crystals, the dispersion curve of the phononic crystals exhibits the bandgap in which the propagation of the waves is prohibited (Jensen, 2003; Montero de Espinosa et al., 1998; M. Sigalas & Economou, 1993). Gaps may appear in a specific direction of the wave vector, but they may also span the entire 2D or 3D Brillouin zone, where the propagation of elastic waves is prohibited for any polarization and any angle of incidence. Thus the structure acts as a perfect mirror at any angle of incidence, prohibiting the propagation of sound waves. this phenomenon is well known for the electronic bandstructure of crystalline materials in solid-state physics. Similar to photonic band gaps, one can tailor the band structure of the phononic or photonic crystals for their potential applications such as guiding, filtering, and multiplexing of the acoustic waves at the level of the wavelength and realize the advanced censors and acusto-optic devices (Pennec et al., 2010).

2.3.1 Origin of the Band Gaps

The absolute bandgap that exists in phononic crystals are the Bragg type gap, which appears at about an angular frequency ω of the order of c/a, where $c \rightarrow$ the velocity of sound in the structure, and $a \rightarrow$ the lattice parameter. The existence of the absolute bandgaps was predicted theoretically (M. S. Kushwaha et al., 1993, 1994; M. Sigalas & Economou, 1993; M. M. Sigalas & Economou, 1992) in various phononic crystals made up of solid components (Vasseur et al., 1998, 2001), or mixed (solid/fluid) components (Montero de Espinosa et al., 1998). The existence of the bandwidth of the gaps strongly depends on the nature of the constituent materials of the photonic crystals, such as its physical characteristics (density and elastic constants) of the inclusion and the matrix, the geometry of the array, the shapes of the inclusion, and the filling factor.

The gap can also be a resonance type that appears at the frequencies below the Bragg limit. It is possible to obtain the absolute gaps at the frequencies one or two orders lower than the Bragg diffraction without increasing the size of the unit cell in the crystal. Such type of gaps can be realized in the local resonant sonic material that is made up of building units which has the localized resonant modes at specific frequencies(Larabi et al., 2007; Liu, 2000). The resonances interact and produce a resonance gap or the flat bands around the corresponding eigenfrequencies. Since these local resonances depend on the characteristics of the scatterer, their frequency position can be tuned by appropriately selecting the parameters of the scatterer. A phononic crystal formed from such components resonantly interacts and produces a flat band or resonant gap around the corresponding eigenfrequencies. Since these localized resonances depend on the properties of the scatterers, their positions in frequency can be tuned by appropriately selecting the properties (elastic or geometric) of the scatterers. Such materials can find several potential applications, especially in the field of sound insulation or in the realization of vibrationless environments for high-precession mechanical systems, negative refraction, or cloaking acoustic metamaterials

2.3.2 Band Gaps as a Function of the Geometrical and Physical parameter

The theoretical models of 2D and 3D phononic crystals based on the plane wave expansion methods have shown that the width of the acoustic bandgap strongly depends on the geometry, composition, and properties of the constituent materials (Khelif & Adibi, 2016). The main feature of a phononic crystal is that it exhibits a stop band in its transmission spectrum, in which the propagation of waves is prohibited. Three types of phononic crystals can be defined, the difference between them lies in the physical properties of inclusions and matrix. In this way,

solid-solid, fluid-fluid, and mixed solid-fluid composite phononic crystals can be defined. The opening of the wide acoustic band gap requires two main conditions. The first is to have a large physical contrast between the inclusion and the matrix, such as density and sound speed. The second is to have an adequate filling factor of inclusion in the matrix unit cell (M. S. Kushwaha et al., 1993; Vasseur et al., 1998). It can be noticed that the forbidden band gap appears in the frequency domain, which is derived from the ratio of the effective sound velocity in the composite material to the lattice parameter value of the periodic array of inclusions. In a two-dimensional solid-solid phononic crystal, the vibration modes can be decoupled between propagation in the plane where the elastic displacement is perpendicular to the cylinder and out-of-plane propagation where the elastic displacement is parallel to the axis of the cylinder. Only longitudinal modes are allowed in fluid-fluid phononic crystals. In mixed phononic crystals, there may be complex vibration modes in mixed phononic crystals, ranging from the longitudinal direction of the fluid to the longitudinal and transverse directions of the solid part.

Table 2.1 Mass density ρ and elastic constants C_{11}, C_{44}, and C_{12} of silicon and epoxy, $c_1 = \sqrt{\frac{c_{11}}{\rho}}$ and $c_t = \sqrt{\frac{c_{44}}{\rho}}$ represent the longitudinal and transverse speed of sound respectively. (Khelif & Adibi, 2016)

Material	$\rho\ (kg/m^3)$	C_{11} $(\times 10^{11} dyn/cm^2)$	C_{44} $(\times 10^{11} dyn/cm^2)$	C_{12} $(\times 10^{11} dyn/cm^2)$	$c_1\ (m/s)$	$c_t\ (m/s)$
Silicon	2,331	16.57	7.962	6.39	8,430	5,844
Epoxy	1,180	0.761	0.159	0.44	2,540	1,161

Here we give an example of one of a 2D solid-solid phononic crystal that deals with the composition, geometry, and nature of the constituent material. The phononic crystal is made of two common materials, silicon, and epoxy. Silicon is a cubic material with a crystallographic axis [001] that is parallel to the direction of propagation while the epoxy is

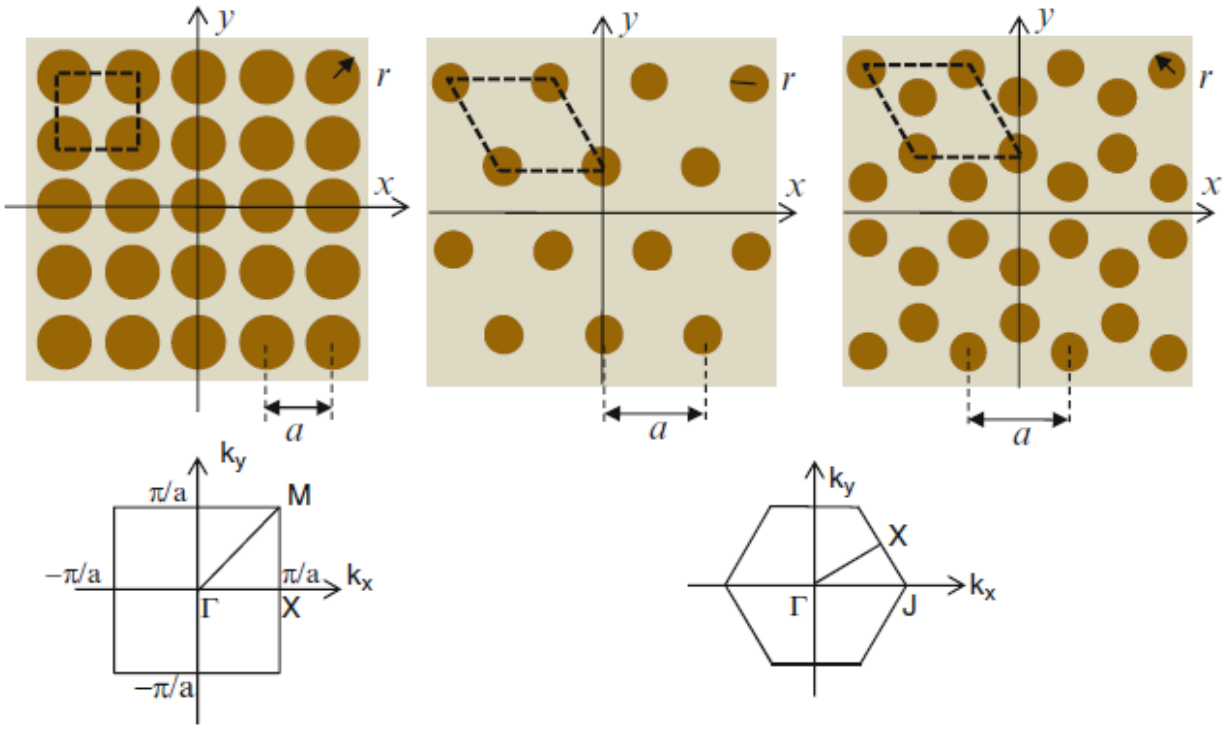

Fig. 2.2 Two-dimensional cross-sections of square, hexagonal, and honeycomb lattices and corresponding Brillouin zones. The dashed lines represent the elementary unit cell of lattice parameter *a*, and *r* is the radius of the inclusions (Khelif & Adibi, 2016).

isotropic (M. S. Kushwaha et al., 1994; Vasseur et al., 1998). The reports of these two materials are given in Table 2.1. it clearly shows the strong contrast between them in their densities and elastic constants indicating that silicon is a hard material compared to epoxy material. This fulfills the first general requirement corresponding to the existence of an absolute bandgap. Fig. 2.2 depicts the three lattices (square, hexagonal, and honeycomb) of the periodic structures. The two-dimensional cross-section of the three arrays under consideration is shown, with *a* representing the lattice parameter. (Γ, X, M) ((Γ, J, X) respectively) are the high symmetry points of the first irreducible Brillouin of the corresponding

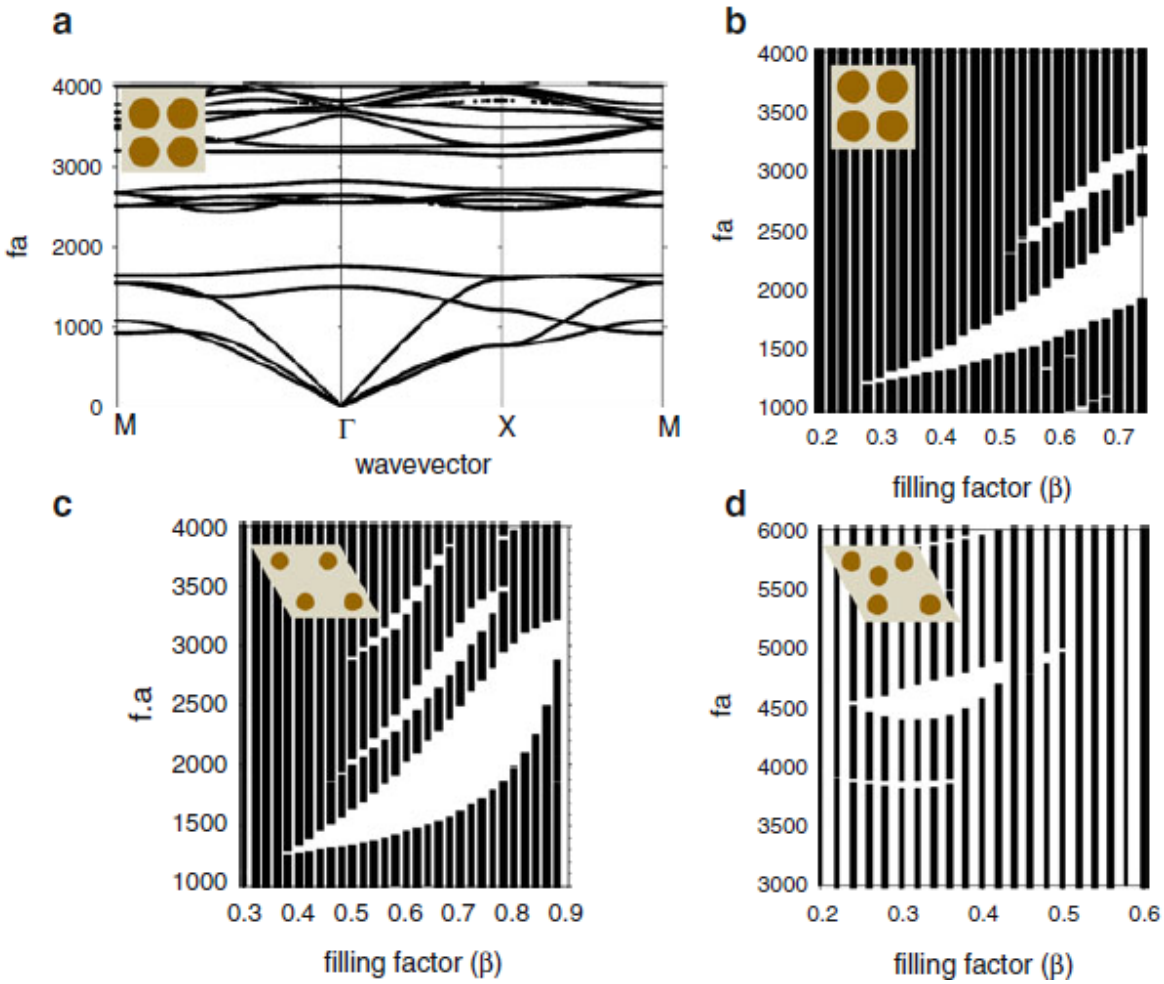

Fig 2.3 Bandgap existence in the phononic crystal made of hard silicon inclusion in the soft epoxy matrix. (**a**) example of dispersion curve for the square array of symmetry with filling factor $\beta = 0.68$. Band gap maps for (**b**) square, (**c**) hexagonal, and (**d**) honeycomb arrays as a function of the filling factors (Khelif & Adibi, 2016).

square (hexagonal and honeycomb) array.Considering first the system with hard materials inclusions inside a soft matrix. Figure 2.3a depicts an example of the dispersion curve of a square array of silicon cylinders in the epoxy matrix, where, β = 0.68 defines the filling factor. Two complete band gaps are observed for the modes in-plane and out-of-plane polarization in the

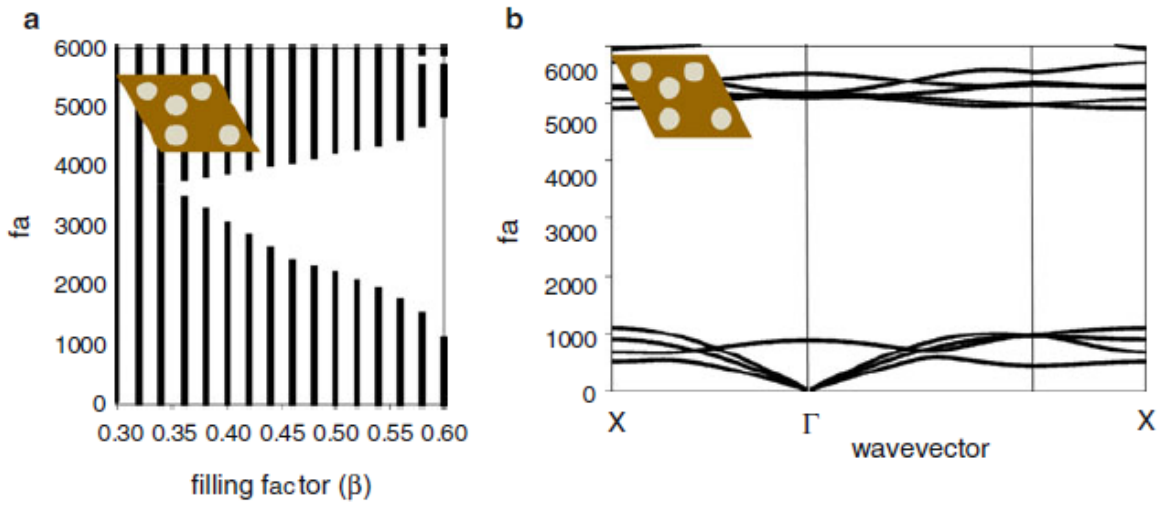

Fig 2.4 (**a**) Bandgap map for the honeycomb array of soft epoxy inclusions in a hard silicon matrix. (**b**) Example of dispersion curves for the honeycomb structure with filling factor $\beta = 0.60$ (Khelif & Adibi, 2016).

frequency spectrum shown in Figure 2.3a. Fig.2.3b shows the evolution of the band gap widths (white area) as a function of the filling factor. The first complete band gap is the largest and is open for a larger range of filling factors (greater than 0.2). It can be seen that the largest width of the band gap ($\Delta(fa)/(fa)_{max} = 28\ \%\ at\ \beta = 0.74$) is open for a very high filling fraction which can be a limitation for technological fabrication.

A second smaller band gap opens for $\beta > 0.55$. With increasing filling factor, the central frequencies of both band gaps increases. The evolution of the band gaps for the hexagonal lattice is presented in Fig. 2.3c. Here the three-band gaps are obtained. The largest gap opens up for a filling fraction of $\beta > 0.36$, with a maximum width ($\Delta(fa)/(fa)_{max} = 37\ \%$) around $\beta = 0.80$.

The representation of the dispersion curve for the honeycomb lattice is given in Fig. 2.3d.

In this lattice, the larger and complete band gap opens at higher frequencies, and for filling fraction in the range $0.24 < \beta < 0.44$. The gap width ($\Delta(fa)/(fa)_{max} = 8\ \%\ at\ \beta = 0.34$) is much smaller than the gap width obtained for the two geometries, in this composite system. One can conclude that for hard inclusions in the soft matrix, the hexagonal and square lattices can obtain the largest band gap, while the former allows lower filling fractions.

We can note that the band gap also depends on the shape of inclusions. For example, it is shown, if the circular inclusion is replaced with the square ones, one can change its position and width. Besides, the band gap can also be adjusted by rotating the square with respect to the axis of the photonic crystal.

In contrast to the case of soft epoxy inclusions in the silicon matrix, square and hexagonal lattices only show absolute band gaps at very high filling rates, which may be of less interest from a manufacturing point of view. On the contrary, for the honeycomb lattice (Figure 2.4), as long as the filling rate exceeds $\beta = 0.34$, the opening of the absolute band gap can be observed. Besides, when $\beta = 0.60$, the band gap width increases sharply and reaches the larger value of $\Delta(fa)/(fa)_{max} = 78\ \%$.

2.4 Effects of non-Hermiticity on Wave Propagation in the Phononic Crystals

Loss is a natural phenomenon, accompanied by multiple energy sources. In terms of acoustics, the loss is usually caused by the impedance mismatch between two contrast media. Since the energy is non-conserved and the information carried by the sound signals is lost. In most cases, the loss is undesired in acoustic wave manipulation (Celli & Gonella, 2015; Hou & Assouar, 2015; Molerón et al., 2016; Zigoneanu et al., 2011). However, tailored losses and wise design of impedance curves can lead to the realization of devices with unconventional

characteristics and novel functions. In recent years, the use of metamaterials (composite materials with specially tailored impedance curves) to control wave propagation has led to many unprecedented technologies. The prospect of using loss or absorption as a key component of metamaterials is becoming a new design methodology.

The most famous example of this non-Hermitian methodology is the creation of even-odd-time symmetric materials. These materials use loss and/or gain to control the propagation of light and sound. New technologies that can emerge from the manipulation of loss and gain include shadowless sensing (Fleury et al., 2015), unidirectional transparency, coherent perfect absorption (Molerón et al., 2016), and asymmetric transmission (Y. Li et al., 2017). Active components are incorporated into these systems through piezoelectric and piezo acoustic effects to provide gain and loss (Christensen et al., 2016; Feng et al., 2017). For example, speakers and non-linear electronic circuits have been used to control the flow of sound. Passive conservative nonlinearity has also been used to achieve asymmetric transmission. In many such conservative non-linear systems, the output signal is collected at a different frequency from the input signal.

The field of non-Hermitian acoustics has risen and has become a hot topic in the field of material science. The field has opened a possibility of making benefits from the engineered loss. The most represented example should be parity-time symmetric acoustic medium, in which the judiciously designed loss gain can lead to one-way reflection as well as the unidirectional cloaking (Cummer & Schurig, 2007; Fleury et al., 2015). Such intriguing phenomena are demonstrated to be closely related to the existence of exceptional points (EPs) in the non-Hermitian systems (Feng et al., 2017). The other examples are the realization of photonic and phononic crystals, modulated and negative refractive index materials, cloaking, and super-

resolution systems have demonstrated the increasing ability to design and manufacture the dielectric and mechanical impedance curves of basic structures that can modify the propagation of waves (light and sound) yielding exotic wave phenomena (Christensen et al., 2016; Feng et al., 2017). It has been shown that the value of non-hermiticity alters the width of the band-gaps. At EPs, the gap between the two bands becomes zero (Ding et al., 2015). With this, it is also possible to manipulate the field propagation only by tuning the loss in the structure utilizing the consequences of changes in the gap width resulting from the non-Hermiticity (Y. Li et al., 2017).

In this thesis, we will demonstrate the effect of non-Hermiticity on the wave propagation in the phononic crystal and utilize this to design a filter that can eliminate the undesired frequencies by absorption in the phononic lattice. Unlike most existing acoustic rectifiers, our design provides a compact system with high-frequency purity that takes advantage of the natural losses of the constituent materials without the need for any external power supply.

2.5 Summary

In this chapter, we have briefly introduced the concept of phononic crystals. Discussed its band structure and the occurrence of the band gaps in its band structures. We demonstrated the dependence of the band gaps on the physical and geometrical parameters with the example of a 2D solid-solid phononic crystal. We have also explored the effects of non-Hermiticity and its influence on the propagation of waves in the phononic crystals. In the next chapter, we will discuss the methods and steps taken to design and simulate our proposed model of a tunable non-Hermitian acoustic filter.

CHAPTER III

PROPOSED MODEL AND STEPS OF SIMULATIONS USING COMSOL MULTIPHYSICS

3.1 Introduction

In this chapter, we will introduce our proposed model and briefly describe the steps taken to simulate the design. We make use of the COMSOL Multiphysics 5.4 software to design and simulate our proposed model. COMSOL Multiphysics is a physics simulation software program that offers numerous physical solvers and the option to couple multiple physics interface modules such as acoustics, electrodynamics, fluid flow, heat transfer, etc (*Multiphysics, C. (1998). Introduction to COMSOL Multiphysics Extregistered. COMSOL Multiphysics, Burlington, MA, Accessed Feb, 9, 2018.*, n.d.). We can build models by defining related physical quantities (such as material properties, loads, constraints, sources, and fluxes) instead of defining basic equations. We can apply these variables, expressions, or numbers directly to solids and fluid domains, boundaries, edges, and points, regardless of the computational grid. The COMSOL Multiphysics software then internally compiles a set of equations representing the entire model. We used the pressure acoustics, frequency domain interface in COMSOL Multiphysics 5.4. to simulate our model. The next part of this chapter will explain the proposed model and simulation steps.

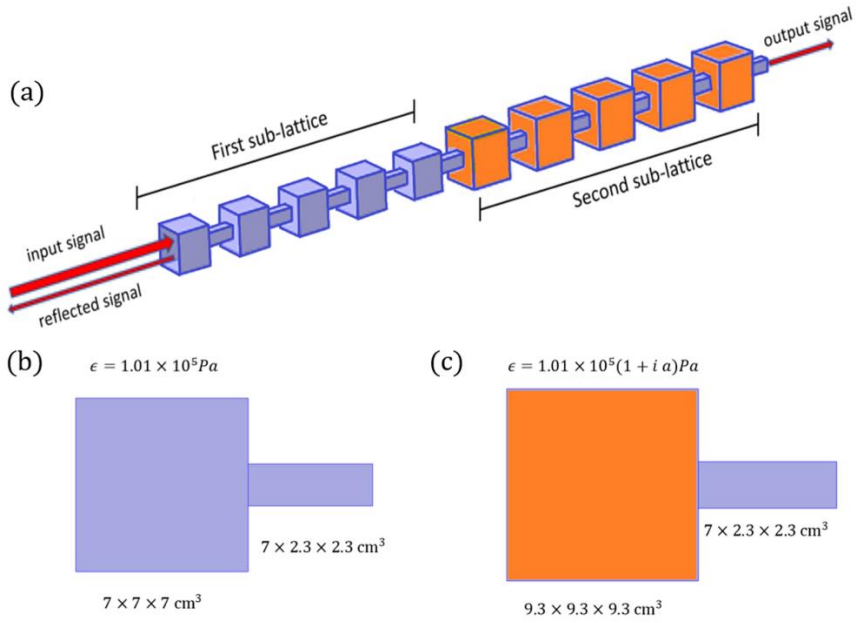

Fig 3.1 (a) Schematic of the super-lattice made of two sub-lattices and works as a tunable acoustic filter. (b) unit cell of the first sub-lattice, (c) unit cell of the second sublattice. The unit cell of the first sublattice consists of a cube and a cuboid of dimensions $7 \times 7 \times 7\ cm^3$ and $7 \times 2.3 \times 2.3\ cm^3$ respectively, and the unit cell of the second sublattice consists of a cube and a cuboid of dimensions $9.3 \times 9.3 \times 9.3\ cm^3$ and $7 \times 2.3 \times 2.3\ cm^3$ respectively. The first sublattice is a Hermitian lattice with a unit cell composed of one square cuboid with $7 \times 7 \times 7\ cm^3$ volume and a rectangular cuboid with $7 \times 2.3 \times 2.3\ cm^3$ volume, both hollow and filled with air having density modulus $\rho = 1.4 \frac{Kg}{m^3}$ and bulk modulus $\epsilon = 1.01 \times 10^5 Pa$. the second sublattice is the non-Hermitian lattice with unit cell composed of hollow cuboids of volume $9.3 \times 9.3 \times 9.3\ cm^3$ and $7 \times 2.3 \times 2.3\ cm^3$, filled with air with the same density modulus and bulk modulus as in the first sublattice except for the bulk modulus of the air in the cuboids of volume $9.3 \times 9.3 \times 9.3\ cm^3$ is $\epsilon = 1.01 \times 10^5 (1 + i\,a) Pa$, with a defining effective loss parameter. The value of a determines the degree of non-Hermiticity in the second sublattice.

3.2 Proposed Model

Our proposed model is a phononic superlattice that consists of twenty hollow cuboids which are connected to each other in a series in the direction of propagation of the acoustic pressure field, *x*. The cuboids are hollow, filled with air, and assumed to be made of polylactic acid (PLA) material. Furthermore, they are either square cuboid, five with $7 \times 7 \times 7$ cm^3 volume in the first sub-lattice, and five with $9.3 \times 9.3 \times 9.3$ cm^3 volume in the second sub-lattice, or rectangular cuboid of volume $7 \times 2.3 \times 2.3$ cm^3 that connects the square cuboids. The schematic of the model is shown in Fig 3.1. In our simulations, we assumed that all the cuboids are made from polylactic acid (PLA), which is hollow and filled with air. The density modulus of air throughout the volume is $\rho = 1.4\ kg/m^3$. We assume the bulk modulus in the rectangular cuboids and the square cuboids of the first sublattice is given by $\epsilon = 1.01 \times 10^5 Pa$, while the effective bulk modulus of the square cuboids in the second sub-lattice is given by $\epsilon = 1.01 \times 10^5 (1 + ia) Pa$. The complex bulk modulus effectively describes the intrinsic or induced material loss and represents the effective loss parameter. We will show in the next chapter that the induced loss in our model can be created using side-holes whose magnitude can be controlled by adjusting the hole dimensions which effectively describes the value of the parameter a. The next section explains the details of the steps of the simulation.

3.3 Steps of Simulations

We follow a simplified workflow to reflect the entire user interface of the software used for the simulation. The modeling workflow can be carried out in the following order: setting up the model environment, building the geometry, specifying the material properties, defining physics boundary conditions, creating the mesh, run simulations, and post-processing of the

simulated results. In the following sections, we will briefly describe each step taken to simulate our proposed model.

3.3.1 Set up the Model Environment

Setting up the model environment is the first step of the simulation. In this step, we add the necessary components to our simulation. From Model Wizard we make selections as a part of our model setup. As our model is three-dimensional, we select the 3D space dimension. The next step is to choose the physics of our simulation. Since we are investigating the acoustic wave propagation through the model, we select the Pressure Acoustics, Frequency Domain (ACPR) within the Acoustic interface. Here the dependent variable is the Pressure denoted as "*p*".

The Pressure Acoustics, Frequency Domain interface is used to compute the pressure variation for the propagation of acoustic waves in fluids at quiescent background conditions. It is suited for all frequency-domain simulations with harmonic variations of the pressure field. The physics interface can be used for linear acoustics described by a scalar pressure variable. It includes domain conditions to model losses in a homogenized way, so-called fluid models for porous materials, as well as losses in narrow regions. Domain features also include background incident acoustic fields, as well as domain monopole and dipole sources. The plane wave attenuation behavior of the acoustic waves may be entered as a user-defined quantity, or defined to be bulk viscous and thermal losses. The physics interface solves the Helmholtz equation in the frequency domain for given frequencies, or as an eigenfrequency or modal analysis study.

After selecting the Physics, we proceed to the "Select Study" section, where we select what we will be calculating in our simulation. Under the "General Studies" section of the Select Study, we find "Eigenfrequency" and "Frequency Domain". The Eigefrequency study is used to

calculate eigenmodes and eigenfrequencies of a linear or linearized model. Whereas the Frequency Domain study is used to compute the response of a linear or linearized model subjected to harmonic excitation for one or several frequencies. In our simulation, we first need to calculate the eigenmodes of our model, based on which, we investigate the response of the model for several frequency ranges. Therefore, use both Eigenfrequency and Frequency Domain in our study, we will discuss it in more detail in the later sections. Now we proceed to the building of geometry.

3.3.2 Build Geometry

Following various steps in the geometry section of the Model Builder toolbar, we construct our model as we have described in section 3.2. The structure is a superlattice that is composed of two sub-lattices. The first sublattice consists of five unit cells, with each unit cell composed of one cube with $7 \times 7 \times 7\ \text{cm}^3$ volume and a cuboid with $7 \times 2.3 \times 2.3\ \text{cm}^3$ volume. Similarly, the second sublattice is composed of five unit cells each having a cube of volume $9.3 \times 9.3 \times 9.3\ \text{cm}^3$ and a cuboid with $7 \times 2.3 \times 2.3\ \text{cm}^3$ volume. The resulting structure forms a superlattice as shown in Fig.3.1. After the construction of the structure, we proceed to specify the materials and materials properties to our model.

3.3.3 Specify Materials and Material Properties

We can assign the materials of our structure by selecting the materials from the in-built materials library within the COMSOL Multiphysics software. By assigning the materials, we specify the material properties from the materials library for specific materials. As described in section 3.2, we assume our model to be made up of polylactic acid (PLA) material and filled

with air throughout the volume. Therefore we specify the boundary or the wall of the structure to be PLA material, and all the domain to be air material.

The COMSOL automatically assigns the property for the selected materials, however, we can also manually modify the properties from the content. In the property section of the material, we define the density modulus of air throughout the volume to be $\rho = 1.4\ kg/m^3$. Furthermore, we assume the bulk modulus in the rectangular cuboids and the square cuboids of the first sublattice is given by $\epsilon = 1.01 \times 10^5 Pa$ while the effective bulk modulus of the square cuboids in the second sub-lattice is given by $\epsilon = 1.01 \times 10^5 (1 + ia) Pa$, the complex bulk modulus effectively describes the intrinsic or induced material loss and represents the effective loss parameter. The complex bulk modulus makes the second sublattice non-Hermitian, where, "*a"* is the effective loss parameter, the value of which defines the degree of non-Hermiticity in the second sublattice.

3.3.4 Define Physics Boundary Conditions

After defining the material properties, next, we define the physics for the model. As now we have a geometry with usable modeling domains and boundaries, we assign mathematical equations to different parts of the model to simulate our physics. To this end, we have selected various parts of the geometry and specified appropriate equations in the physical conditions describing these parts. For our model, we configure physics for the pressure acoustics, frequency domain interface. All boundary conditions except input and output ports we assume to be sound hard boundary or wall. By this, we mean in constant fluid density ρ_c the normal derivative of the pressure is zero at the boundary, $\frac{\partial p_t}{\partial \mathbf{n}} = 0$. The input and output ports are the radiation boundary condition for the Plane Wave.

3.3.5 Creating Mesh

After the boundary conditions are defined, we create the mesh for the simulation. We choose the physics-controlled mesh, which automatically generates the mesh adapted to the physics on the model. The COMSOL automatically generates the mesh for the pressure acoustics frequency-domain study, the physics that we have defined for our model. We can also opt for the user control mesh and manually control the mesh generation with different element types. Here we use the default physics-controlled mesh for our simulation.

After the mesh is created we then run the simulation followed by post-processing of the results obtained from the simulations. We will discuss running the simulation and the processing of the results in the next chapter. In the next chapter, we will discuss the results obtained from the simulations. We will calculate the eigenfrequencies for both the sublattices and analyze their band structures. We will also see the effect of induced loss or the non-Hermiticity in the bandstructure of the second sublattice. Based on the eigenfrequencies calculated for the model, we will analyze the propagation of the incident frequencies in the particular range by studying the reflection spectra for the range of frequencies incident to the input port.

3.4 Summary

In this chapter, we introduced our proposed model and discussed the steps taken to simulate our model using the COMSOL Multiphysics software. We first introduced our proposed model that will result in a tunable acoustic filter. The model is a superlattice formed by the superposition of two sublattices. The first sublattice is passive or Hermitian whilst the second sublattice is either Hermitian or non-Hermitian depending on the value of effective loss parameter a, in the nonzero imaginary bulk modulus.

Next, we described the steps of simulations beginning with setting up the model environment followed by building geometry and specifying the materials and material properties. Then we defined the physics for the model and the appropriate boundary conditions for the simulation. We also generated the appropriate mesh that is adapted to the physics on the model for running the simulation. After the mesh is created we then run the simulation followed by post-processing of the results obtained from the simulations. The next chapter will discuss running the simulation and the processing of the results.

CHAPTER IV

SIMULATED RESULTS AND THE REALISTIC MODEL

4.1 Introduction

As we discussed in the previous chapter, we assigned physical and boundary conditions to the model in order to simulate our model. We configured the pressure acoustics, frequency domain interface for the model. In this chapter, we will briefly discuss pressure acoustics, the frequency domain. Using the pressure-acoustic interface in COMSOL, we will study the eigenfrequencies and calculate the band structure of the model. On this basis, we will also study the signal propagation in a specific frequency range by analyzing the reflection spectrum of the signal incident through the input port of the phononic crystal. Then, we will study the influence of non-Hermiticity in the band structure and the signal propagation due to the induced loss in the second sub-lattice, and observe the filtering of specific frequency signals. Finally, we will introduce a realistic model in which we will devise square holes on the facets of the larger cuboids in the second sublattice and perform the same simulation as before. At this time, assuming the bulk modulus of the air in all cuboids of both sublattices (including the larger cuboids in the second sublattice) is real, and the results are compared with the theoretical model.

4.2 Pressure Acoustics, Frequency Domain

The Pressure Acoustics Frequency Domain interface is designed to analyze various types of pressure acoustic problems in the frequency domain, all of which are related to pressure waves

in the fluid. The acoustic model is part of a larger multiphysics model that can describe the interaction between structures and sound waves. This physical interface is suitable for modeling acoustic phenomena that do not involve fluid flow. This interface solves for the acoustic pressure, p.

4.2.1 Frequency Domain Study

The frequency-domain or time-harmonic formulation uses the following inhomogeneous Helmholtz equation (Givoli & Neta, 2003):

$$\nabla.\left(-\frac{1}{\rho_c}\left(\nabla_p - \boldsymbol{q}_d\right)\right) - \frac{\omega^2 p}{\rho_c c_c^2} = Q_m \qquad 4.1$$

In this equation, $p = p$ (**x**, ω) (the dependence on ω is henceforth not explicitly indicated). Q_m (SI unit: $1/s^2$) represents the monopole source and $\boldsymbol{q}_\mathrm{d}$ represents the dipole source (SI unit: $N/m\text{^}3$). With this formulation, you can compute the frequency response of a system for a number of frequencies. The default frequency-domain study sets up a parametric sweep over a frequency range using a harmonic load. When there is damping, ρ_c and c_c are complex-valued quantities.

4.2.2 Eigenfrequency Study

In the eigenfrequency formulation, the source terms are absent, and the eigenmodes and eigenfrequencies are solved for (Givoli & Neta, 2003):

$$\nabla.\left(-\frac{1}{\rho_c}\nabla_p\right) + \frac{\lambda^2 p}{\rho_c c^2} = 0 \qquad 4.2$$

The eigenvalue λ introduced in this equation is related to the eigenfrequency f and the angular frequency ω, through $\lambda = i2\pi f = i\omega$. Because they are independent of the pressure, the solver ignores any dipole and monopole sources unless a coupled eigenvalue problem is being solved.

4.3 Simulated Results and Discussion

In this section, we will discuss the simulated results obtained for the model shown in Fig. 3.1 (a). We will analyze the band structures of each sublattice. Later we will also study the field propagation by analyzing the reflection curve obtained when the signal of a certain frequency range is incident to the input port of our model.

4.3.1 Bandstructures

We plotted in Fig.4.1 (a) the band structure of an infinite passive lattice with a unit cell similar to the passive sub-lattice. In contrast, Figs.4.1 (b),(c) show the band structure of an infinite non-Hermitian lattice with the same unit cell as the one in the non-Hermitian sublattice in Fig.3.1(a) and with $a = 0$ and $a \neq 0$, respectively. A comparison between Fig.4.1 (a),(b) shows that in the frequency range $0\ Hz - 265\ Hz$ there is a partial overlap between the first passband of the two lattices. Thus, we expect that if the frequency of the incident field in Fig. 4.1 lies in this range of frequency, namely $0\ Hz - 265\ Hz$, it will pass through both super-lattices without any absorption. However, if the imaginary part of the bulk modulus of the large cuboids of the second lattice, namely non-Hermitian one, is equal to zero i.e. $a = 0$, in the frequency range $265\ Hz - 407\ Hz$, highlighted with an orange ribbon in the upper panel of Fig.4.1, where the passive lattice has a passband the second sub-lattice has a bandgap. Thus, we anticipate that for $a = 0$ any incident field in the frequency range $265\ Hz - 407\ Hz$, gets reflected from the

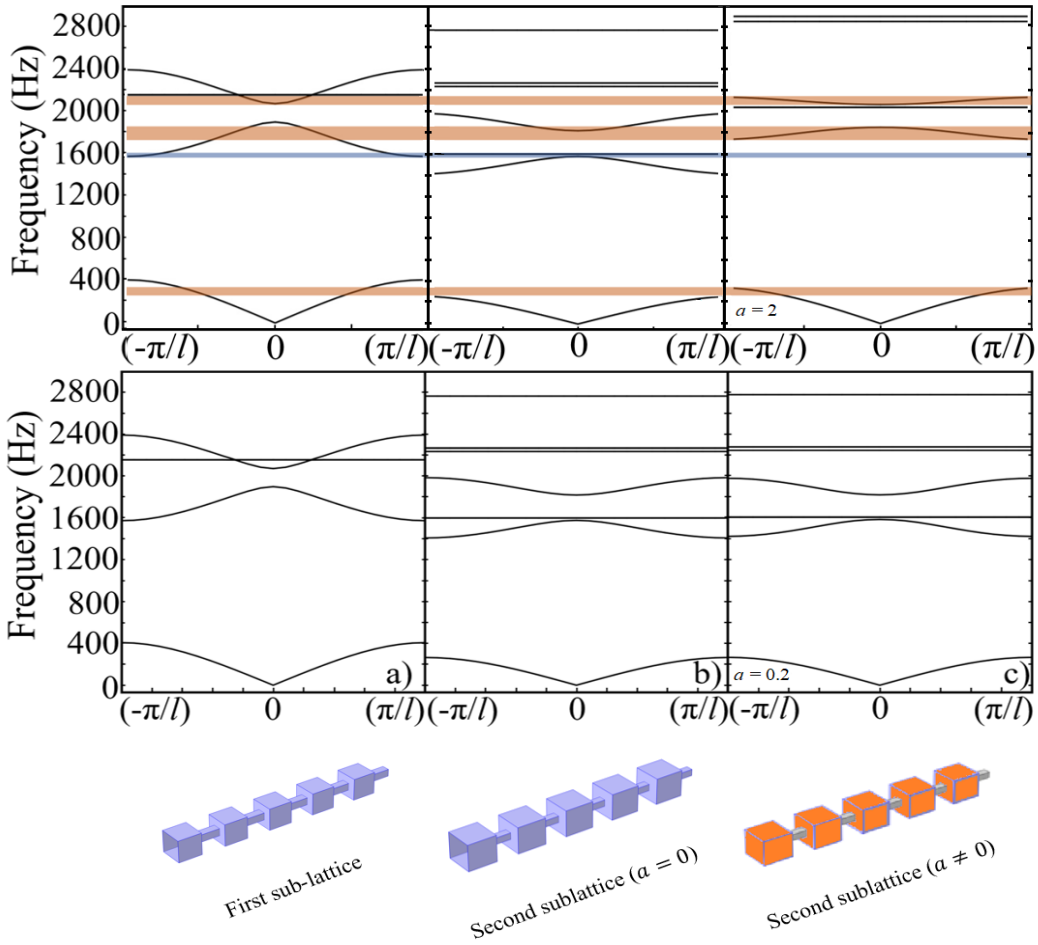

Fig. 4.1. Schematic of the band structure of each sub-lattices. The first bandstructure is for the **(a)** first (passive) sub-lattice followed by the band structures of the second sublattice when **(b)** $a = 0$ and **(c)** $a \neq 2$ respectively. The lower passband of the passive sub-lattice has partial overlap with the passband of the second sub-lattice when $a = 0$. Thus the frequency window that is not placed at the pass-band of the two sub-lattice gets reflected. The lower passband of the lossy sub-lattice moves upward with the increase of the effective loss parameter to $a = 2$ in the larger cubes of the second sublattice. However, in a realistic case, the largest value of loss that can be achieved is $a = 0.2$, and we see such a small amount of a has a tiny effect on the band structure of the phononic lattice.

second sub-lattice. A similar scenario occurs for the second passbands where there is a small overlap between the passband of the first and second sub-lattices in the frequency range $1572\ Hz - 1575\ Hz$ which is highlighted with a light blue ribbon shown in the upper panel of Fig.4.1. Notice that there is a partial overlap between the second band of the first sub-lattice and the third pass-band of the second sub-lattice in the frequency range $1817\ Hz - 1897\ Hz$. However, in this frequency range, the overlapping occurs at the center of the band structure with wave numbers close to zero. The bands are almost flat and the group velocity becomes very small. Therefore we expect small transmission and large reflection at this frequency range. The third passband of the first sub-lattice is located at frequencies that the second sub-lattice has a gap, namely $2070\ Hz - 2390\ Hz$. Thus, we expect reflection with zero transmission at these frequencies when $a = 0$.

Now let us consider the effect of increasing losses in the second sublattice. Our simulation shows the significant changes in the bandgap of the second sublattice when the value of the effective loss parameter is $a = 2$ (Fig. 4.1(c) upper panel). However, the value $a = 2$ is very large and not achievable for practical use. Our simulation for the realistic model, which we will discuss in the later sections, shows that the largest value of loss that we could achieve is in the order of $a \approx 0.2$. As we can see in Fig. 4.1 (c), such a small amount of a has a tiny effect on the band structure of the phononic lattice. Consequently, one might naively claim that the addition of the loss will not affect the dynamics in the system and the only observation might be the addition of trivial absorption in the reflected or transmitted signal. In the next section, we will show that surprisingly this picture is not true and the addition of loss can result in the generation of additional resonances. While we use the generated resonances to develop a tunable filter, one

might potentially use these resonances for designing tunable modulators based on non-Hermiticity.

4.3.2 Reflection Curves of the Combined system

We have plotted the reflection of our lattice in the lower panel of Fig. 4.2 for $a = 0$ (blue curve) and for $a = 0.2$ (red curve) using the full-wave simulation where the reflection amplitude $R = \left|\frac{W_R}{W_{in}}\right|^2$, with

$$W_{in} = \int_{S_{2(1)}} \frac{|P_0|^2}{2\rho c}, W_R = \int_{S_1} \frac{|P_0 - P|^2}{2\rho c} \qquad 4.3$$

In Eq.4.3 $P_0, P, \rho,$ and c are amplitude of incoming pressure wave, total pressure wave, density, and speed of sound, respectively. S_1 is the surface containing the pressure flux at the input port in Fig. 4.2 (upper-left panel).

We observe in the frequency range $0\ Hz - 265\ Hz$ the reflection peaks are smaller when $a \neq 0$. As depicted in Fig.4.2 at frequency ranges that the two sublattices have band-gap or the first sub- lattice has bandgap we expect to have complete reflection irrespective of the value of a. This matches our simulation in Fig.4.2.

Now let us focus on the frequency ranges where the first sub-lattice has a passband but the second sub-lattice has a band-gap. For instance, in the frequency range 265 Hz-410 Hz the first sub-lattice has a passband and the second one has a gap irrespective of the value of a. Thus, we expect that due to the gap of the second sublattice we have a total reflection. In Fig.4.2 and for $a = 0$ the blue curve shows that our intuition is correct and we have a total reflection. However, for $a \neq 0$, see the red curve, there are two resonances and consequently, we do not have a full reflection. The same scenario occurs in other frequencies that the gap of the second sub-lattice

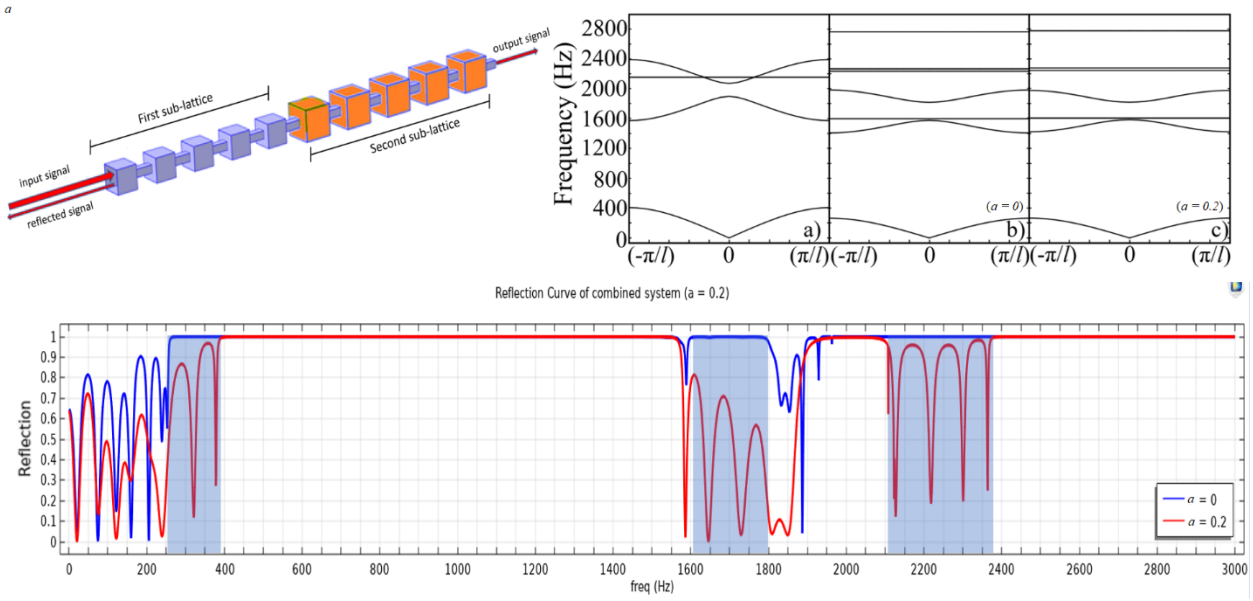

Fig 4.2. (Lower panel) Reflection curve of the super-lattice shown in upper-left panel, for $a = 0$ (blue curve) and $a = 0.2$ (red curve). For several frequencies in different frequency windows, we observe a large contrast in the reflection when we increase the value of parameter a, even though we don't see any significant difference in the bandstructure when the loss parameter is increased to $a = 0.2$ (upper-right panel).

overlaps with the passband of the first sub-lattice. The existence of such resonances is the main ingredient of our proposed filter. By introducing the non-Hermiticity we can remove specific frequencies from the reflected field. The benefit of our proposed system is in the existence of such sharp resonances which allow for a very precise filtering process.

4.3.3 Scattering Formula

To understand the source of the new resonances that are appearing in the reflection curve due to the non-Hermiticity let us look at the scattering matrix associated with our system. The transfer matrices of the first sub-lattice, M_1, and second sub-lattice, M_2, as a function of the reflection and transmission coefficient of each sub-lattice, are given by

$$M_1 = \begin{pmatrix} t_1 - \frac{r_1^2}{t_1} & \frac{r_1}{t_1} \\ -\frac{r_1}{t_1} & \frac{1}{t_1} \end{pmatrix}, M_2 = \begin{pmatrix} t_2 - \frac{r_2^l r_2^r}{t_2} & \frac{r_2^r}{t_2} \\ -\frac{r_2^l}{t_2} & \frac{1}{t_2} \end{pmatrix} \quad 4.4$$

Above, t_1, r_1 are the transmission and reflection coefficient of the first sub-lattice and t_2, r_2^l, r_2^r are the transmission, left reflection, and right reflection coefficients of the second sub-lattice respectively. Notice that for the second sub-lattice r_2^l might not be equal to r_2^r when $a \neq 0$. We can multiply the two above matrices and find the total transfer matrix $M = M_2 \times M_1 = \begin{pmatrix} m_{11} & m_{12} \\ m_{21} & m_{22} \end{pmatrix}$ of our structure. Specifically, M-matrix is given by

$$M = \begin{pmatrix} \frac{(r_1^2 - t_1^2)(r_2^r r_2^l - t_2^2) - r_1 r_2^r}{t_1 t_2} & \frac{r_2^r(1 - r_1 r_2^l) + r_1 t_2^2}{t_1 t_2} \\ -\frac{t_1^2 r_2^l - r_1^2 r_2^l + r_1}{t_1 t_2} & \frac{1 - r_1 r_2^l}{t_1 t_2} \end{pmatrix} \quad 4.5$$

The transmission, t, left and right reflection, r^l, r^r, coefficients of our 1D lattice are related to the elements of the transfer matrix

$$t = \frac{1}{m_{22}}, r^l = -\frac{m_{21}}{m_{22}}, r^r = \frac{m_{12}}{m_{22}} \quad 4.6$$

and thus the left reflection in our system will be given by

$$r^l = \frac{r_2^l(t_1^2 - r_1^2) + r_1}{1 - r_1 r_2^l} \quad 4.7$$

We can use Eq.(4.7) to explain the total reflection on the left side of our structure for different scenarios of band structures in the two sub-lattices. For example, if the incident field is at the frequency which the first lattice has a gap, then $r_1 = 1, t_1 = 0$ and consequently $r^l = \frac{-r_2^l + 1}{1 - r_2^l} = 1$, which means no matter if the frequency of the incident field is in the band or gap of the second

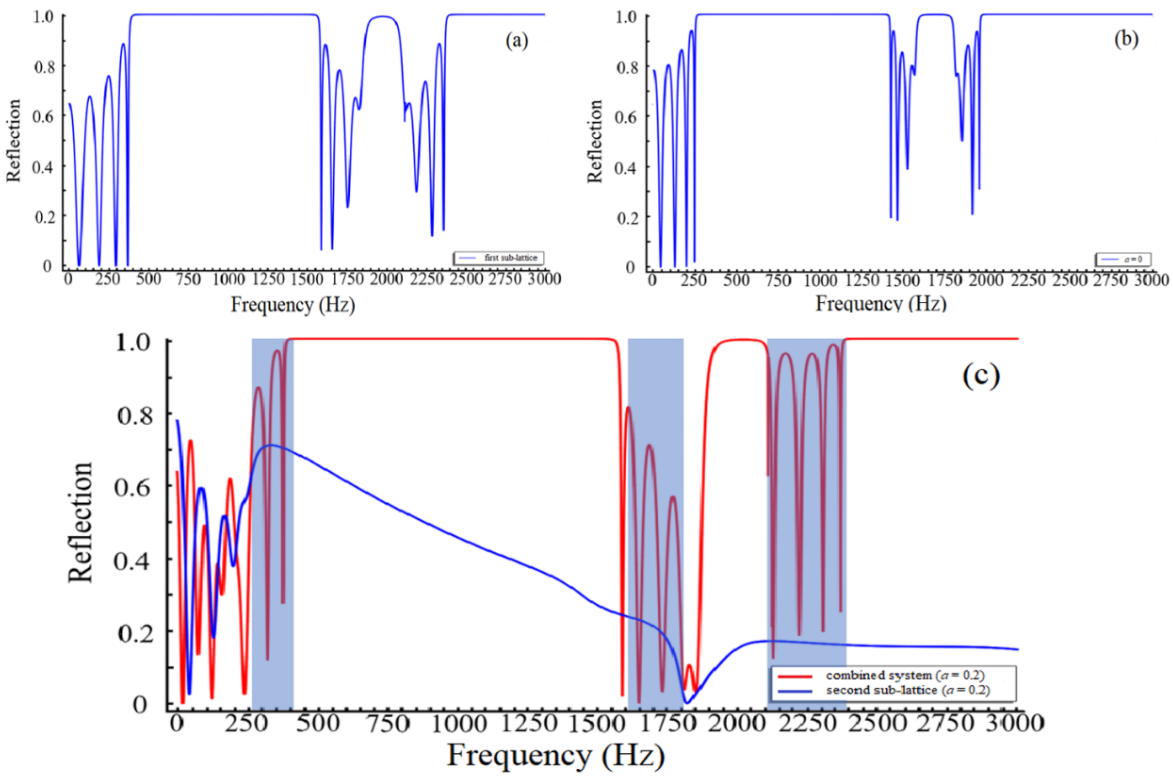

Fig. 4.3 Reflection curves of **(a)** first sub-lattice, and second sub-lattice when the effective loss parameter **(b)** $a = 0$, and **(c)** $a = 0.2$ (blue curve). For guiding the eyes of the reader in **(c)** we plotted also the reflection from the left of the combined structure and highlighted the new peaks (red curve).

sub-lattice, we get the total reflection. Now, let us consider a case that the incident field frequency is in the passband (gap) of the first (second) sub-lattice. To simplify the analysis let us assume that the frequency of the incident beam is at the resonance of the first sub-lattice and thus $r_1 = 0, t_1 = 1$. In this case, Eq.(5) simplify to $r^l = r_2^l$. This means that when $a = 0$ we get a total reflection, however, when $a \neq 0$ the r_2^l would not be equal to one due to the absorption. For strong absorption, we can completely remove the reflection at certain resonance frequencies of the first sublattice. Here it becomes clear that why having the first sub-lattice is useful. It generates resonances and thus allows us to have accurate filtering of certain frequencies.

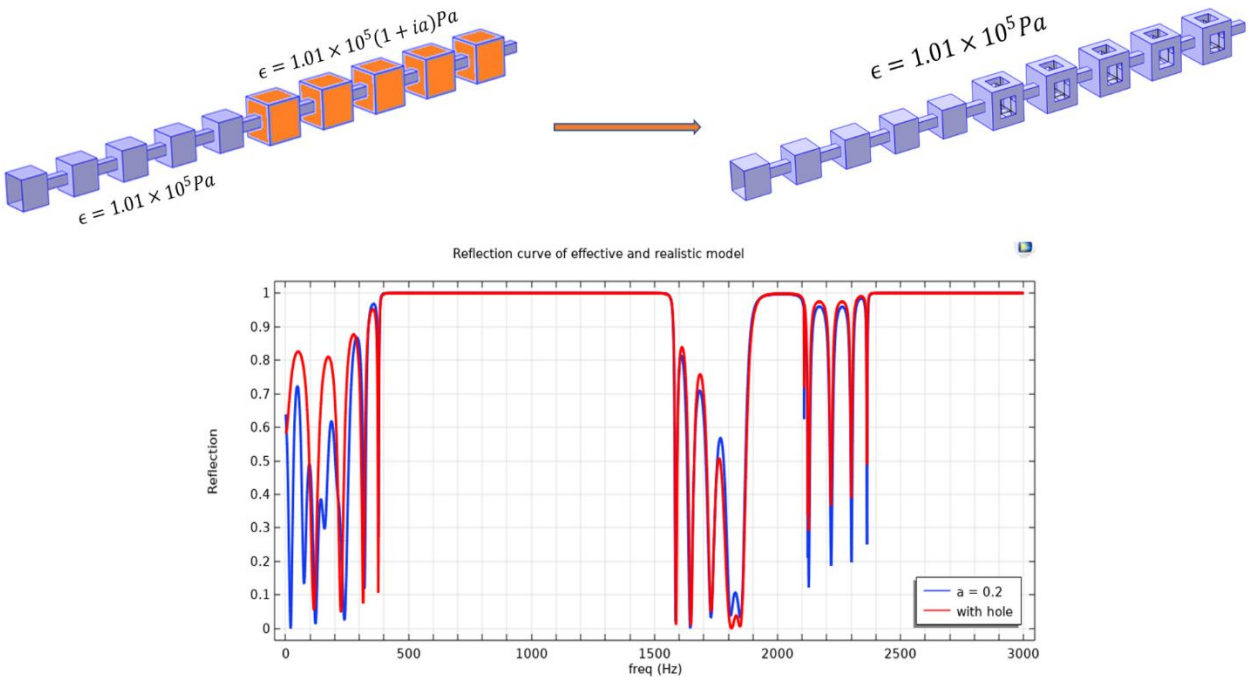

Fig. 4.4 Schematic of the realistic model (upper-right panel) where we assumed large cuboids in the non-Hermitian (lossy) section have the same bulk modulus as the passive section and we devised square holes with sides (s = 4.6cm) in large cuboids. (lower panel) Comparison of the reflection amplitude from the realistic model (structure with embedded holes, red curve) and effective model with a = 0.2 (blue curve). We observe that in the frequency range(406 – 3000)Hz the two models match each other.

Furthermore, by engineering the geometry of the first sub-lattice we can design the number of resonances as well as their positions.

To support the above theoretical analysis we provided the reflection associated first sub-lattice and second sublattice with $a = 0$ and $a = 0.2$ and the r^l for the combined system in Fig.4.3.

4.3.4 The Realistic Model

As it was mentioned before, for the purpose of simulation we assumed an effective and constant imaginary part of the bulk modulus a of air in the system in the second sub-lattice which does not depend on frequency. However, in more realistic situations the parameter a is frequency-dependent. To indicate the effect of frequency-dependent losses and have a more realistic simulation in our tunable filter we introduced square holes with the side length, $s = 4.6\ cm$ on each facet of the last five square cuboids. We performed the same simulation as before while this time we assume that the air in all larger cuboids has the real bulk modulus ($\epsilon = 1.01 \times 10^5 Pa$). The lower panel in Fig.4.4 compares reflections associated with the structure with the holes (red curve) and effective bulk modulus model when $a = 0.2$. We observe that the effective model nicely matches the more realistic model.

4.4 Summary

In this chapter, we discussed the pressure acoustics, frequency domain in the COMSOL and calculated the band structures of the infinite lattices having the unit cells similar to the sublattices of our model. Analyzing the bandstructure we also investigated the acoustic field propagation in the superlattice by studying the reflection of the superlattice. By introducing the non-Hermiticity in the second sublattice, in the form of a complex bulk modulus, we were successfully able to eliminate the signal of certain frequencies and achieve the filter. We designed the realistic model in which we introduced square holes on each facet of the last five square cuboids to include the effect of frequency-dependent losses and have a more realistic simulation in our realistic model. The simulation results show the realistic model is consistent

with the theoretical/proposed model, and therefore we are able to achieve a tunable non-Hermitian acoustic filter.

CHAPTER V

INVESTIGATION OF MODE PROPERTIES IN NON-HERMITIAN SYSTEM OF COUPLED ACOUSTIC RING RESONATORS

5.1 Introduction

In this chapter, we study the geometry-induced non-Hermitian mode couplings and study the different modes in a system of non-Hermitian acoustic ring resonators. We propose and design a system of coupled ring resonators and analyze the eigenmodes of the system. We study the eigenfrequencies and the corresponding pressure field we analyze the localization of the field within the system. In the next sections, we will introduce and investigate different modes in a coupled ring resonators.

5.2 Designing the Coupled Ring Resonators

We designed the ring resonator using the model wizard in COMSOL Multiphysics, following similar steps as explained in chapter 3. The schematic of the proposed structure that we used in our simulation is depicted in Fig. 5.1. We design a resonator that is formed by coupling ten ring resonators, each of inner and outer radius as $r_1 = 37\ cm$ and $r_2 = 42\ cm$ respectively. The thickness of the structure is $t = 5\ cm$, such that the cross-section of hollow space within the resonator is $5\ cm \times 5\ cm$. Among the ring resonators, a resonator in one of the ends encloses an S-shaped waveguide with tapered ends. Similar to our acoustic filter model, we assume the resonators to be made of polylactic acid (PLA) material and the hollow space within the structure

is filled with air. The density modulus and the bulk modulus of the air contained within the resonators are given by $\rho = 1.4\ kg/m^3$ and $\epsilon = 1.01 \times 10^5 Pa$ respectively. We assume the tapered end of the S-shaped waveguide to be lossy and we introduce a complex bulk modulus, $\epsilon = 1.01 \times 10^5 (i + a) Pa$, for the air, contained in the tapered end of the S-shaped waveguide, where a is the effective loss parameter. The value of loss parameter a defines the degree of non-Hermiticity of our coupled system. Similar to the previous model of tunable acoustic filter that we discussed in previous chapters, the larger the value of a, the larger the non-Hermiticity.

5.3 Setting up Model for Simulations

We follow the similar workflow that we followed to simulate our acoustic filter model in COMSOL Multiphysics that we discussed in the previous chapters. We select the 3D space dimension in Model Wizard to set up our model. Again we are investigating the behavior of acoustic waves in the model, we select the Pressure Acoustics, Frequency Domain (ACPR) within Acoustic Interface. The details of the pressure acoustics, frequency domain have been already discussed in chapter 3.

After the model is set up, we build the geometry. Our proposed structure is a set of ten ring resonators that are connected and coupled. Each ring resonators have the inner and outer radius of $r_1 = 37\ cm$ and $r_2 = 42\ cm$ respectively. The thickness of the structure is $t = 5\ cm$, such that the cross-section of hollow space within the resonator is $5\ cm \times 5\ cm$. Among the ring resonators, a resonator in one of the ends encloses an S-shaped waveguide with tapered ends. The S-shaped waveguide has a cross-section similar to the other ring resonator. Similar to our acoustic filter model, we assume the resonators to be made of polylactic acid (PLA) material and the hollow space within the structure is with air.

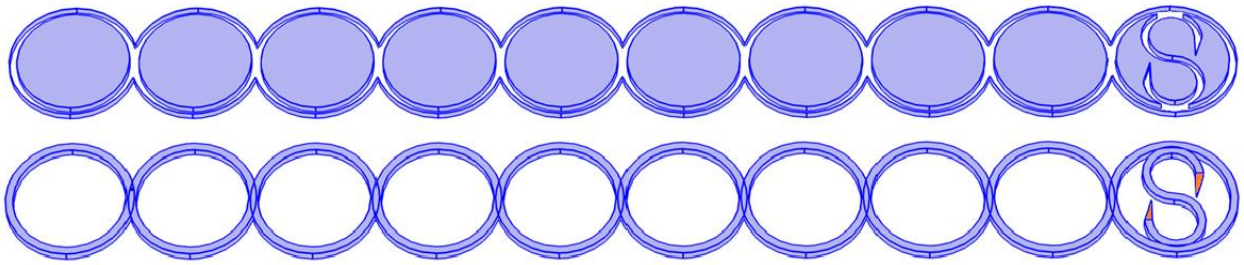

Fig.5.1 Schematic of the model formed by coupling ten ring resonators. A resonator at the end encloses an S-shaped waveguide with tapered ends and is coupled with the ring resonator enclosing it. The structure is made of polylactic acid (PLA) material (upper panel). The hollow space is filled with air material (lower panel). The inner and outer radius of each resonator is $r_1 = 37\ cm$ and $r_2 = 42\ cm$ respectively. And the thickness of the structure is $t = 5\ cm$, such that the cross-section of hollow space within the resonator is $5\ cm \times 5\ cm$. the density modulus and the bulk modulus of the air that fills the hollow space is $\rho = 1.4\ kg/m^3$ and $\epsilon = 1.01 \times 10^5 Pa$ respectively. The air within the tapered end of the S-shaped waveguide (the orange region in lower panel) as $\epsilon = 1.01 \times 10^5(1 + ia)Pa$, where a is the effective loss parameter. The complex bulk modulus describes the intrinsic or the induced material loss making the system non-Hermitian or Hermitian depending on the value of a.

We assume the structure of our model is made up of polylactic acid (PLA) material and is filled with air within the hollow space. Therefore, we specify the boundary or the wall of the structure as the PLA material and the domain which we assume to be hollow to be air, from the materials library within the COMSOL Multiphysics software. We define the density modulus and the bulk modulus of the air material to be $\rho = 1.4\ kg/m^3$ and $\epsilon = 1.01 \times 10^5 Pa$ respectively, in the materials property section. As we want the tapered end of the S-shaped waveguide to be lossy

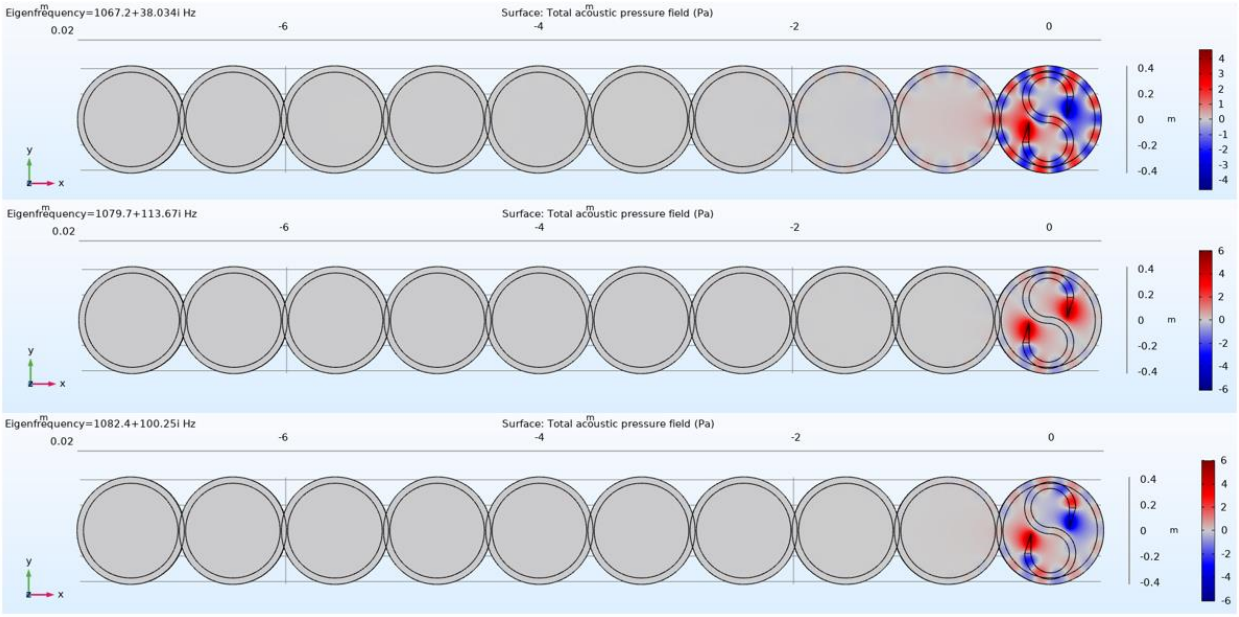

Fig.5.2 Schematic of the pressure fields for a system with loss parameter $a = 2$. The figure shows strong localization of fields in the frequencies $1067.1 + 38.07i\ Hz, 1079.7 + 113.67i\ Hz$, and $1082.4 + 100.25i\ Hz$ when $a = 2$.

we define the complex bulk modulus for the air within the tapered end of the S-shaped waveguide as $\epsilon = 1.01 \times 10^5(1 + ia)Pa$, where a is the effective loss parameter. The complex bulk modulus describes the intrinsic or the induced material loss making the system non-Hermitian or Hermitian depending on the value of a. Larger the value of a, the higher degree of non-Hermiticity.

We define all the boundary conditions to be a sound hard boundary. Since here we will be studying the eigenfrequency only, therefore, we do not define port at the time. After all the parameters are defined we generate mesh for our simulation. Likewise, we define the extra-fine mesh for our simulation by manually generating the mesh for our pressure acoustics frequency-domain study.

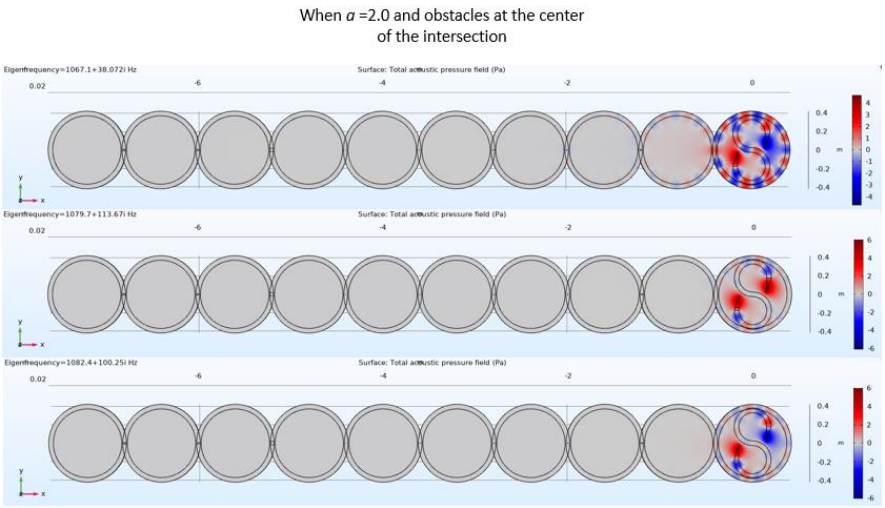

Fig.5.3 Schematic of the pressure fields for a system with loss parameter $a = 2$ and with obstacles at the center of the intersection of each resonator. The figure shows strong localization of fields in the frequencies $1067.1 + 38.07i\ Hz, 1079.7 + 113.67i\ Hz$, and $1082.4 + 100.25i\ Hz$ when $a = 2$.

5.4 Simulations and Results Discussion

We did the simulation to study the different modes in our system after setting up the model. We did the eigenfrequency study and plotted the pressure fields for various eigenfrequencies in the structure. At first, we simulated for the non-Hermitian system with effective loss $a = 2$. Our simulation showed (Fig. 5.2) the strong localization of the pressure fields in the frequencies; $1067.1 + 38.07i\ Hz, 1079.7 + 113.67i\ Hz$, and $1082.4 + 100.25i\ Hz$. Then, we introduced obstacles of random size in the center of the area where the resonators intersect each other, except at the intersection point connecting the ring resonator, which surrounds the S-shaped waveguide, and performed the same simulation as before. We analyzed the pressure fields for different eigenfrequencies. We obtained the pressure field location at the same frequency as before. The localized pressure field is not affected by

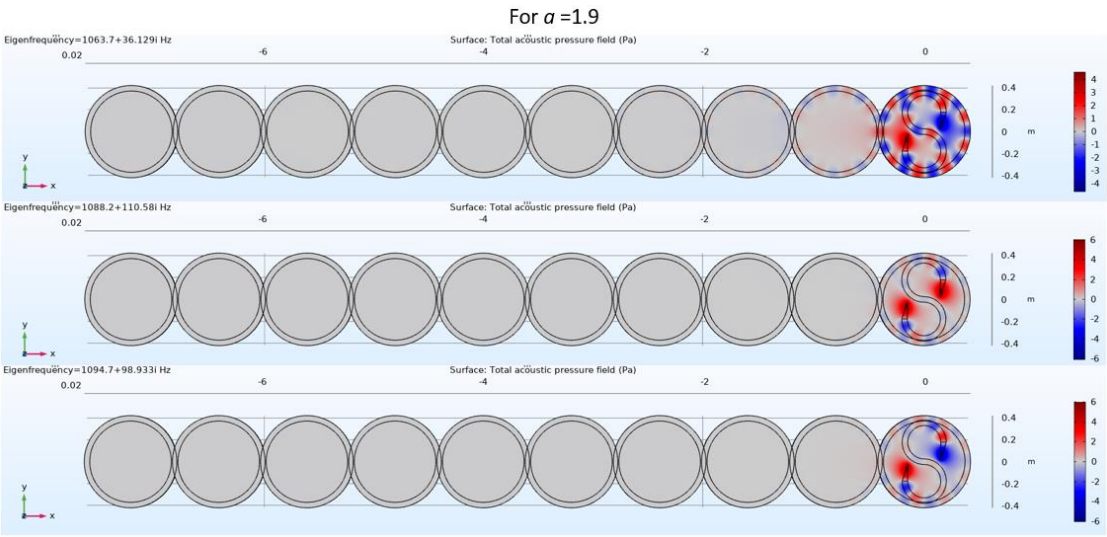

Fig.5.4 Schematic of the pressure fields for a system when loss parameter $a = 1.9$. The figure shows strong localization of fields in the frequencies $1063.7 + 36.329i\ Hz, 1088.2 + 110.58i\ Hz$, and $1094.7 + 98.933i\ Hz$ when $a = 1.9$.

obstacles, as shown in Figure 5.3. Regardless of whether there are obstacles in the system, the positioning of the magnetic field in the frequencies of $1067.1 + 38.07i\ Hz, 1079.7 + 113.67i\ Hz$, and $1082.4 + 100.25i\ Hz$ is robust.

In addition, we studied the effect of decreasing value of loss parameter a on the behavior of the localized field in the system. We simulated in the descending order of the loss parameter value a from $a = 2.0$ to $a = 0$, with an interval of 0.1. Figure 5.3 to Figure 5.22 depict the simulation results for the different values of the loss parameter a. Table 5.1 reports the field localization observed for the loss parameter value $a = 2.0\ to\ a = 0$ in decreasing order. For different values of a, we observe the localization in different frequencies. Or in other words, we can say that the localization shifts to the different frequencies by changing the order of the non-Hermiticity. In addition, we can see that when the system is Hermitian (i.e. $a = 0$), we only observe the field localization in the frequencies of 1017.9 Hz and 1059.5 Hz. However, we were

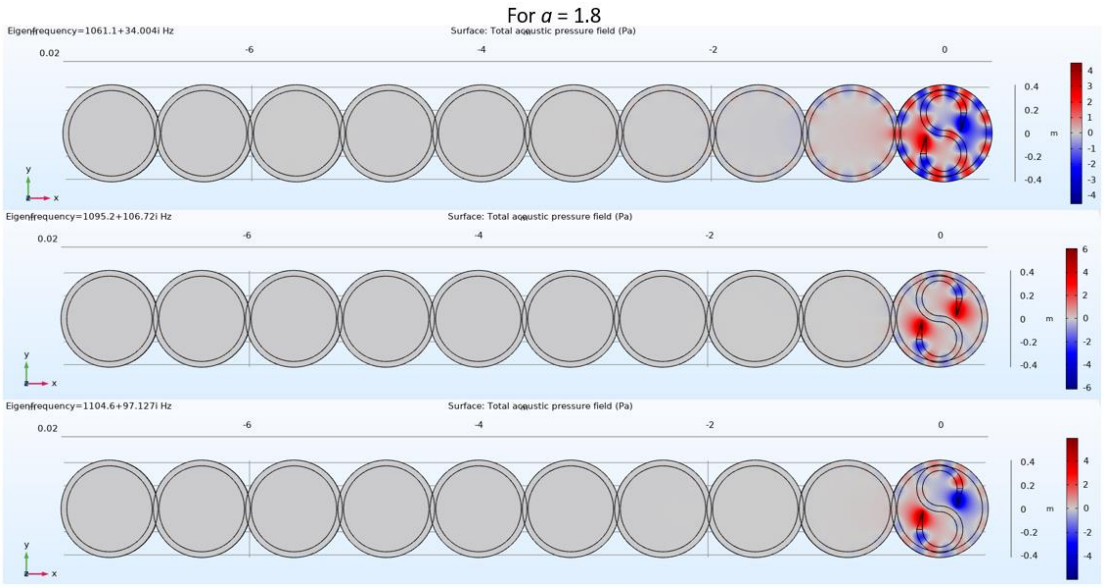

Fig.5.5 Schematic of the pressure fields for a system with loss parameter $a = 1.8$. The figure shows strong localization of fields in the frequencies $1061.1 + 34.004i\ Hz, 1095.2 + 106.72i\ Hz$, and $1104.6 + 97.127i\ Hz$ when $a = 1.8$.

able to obtain three localization when the system is non-Hermitian (or when $a \neq 0$). Our results suggest the tunability in localization of the pressure field.

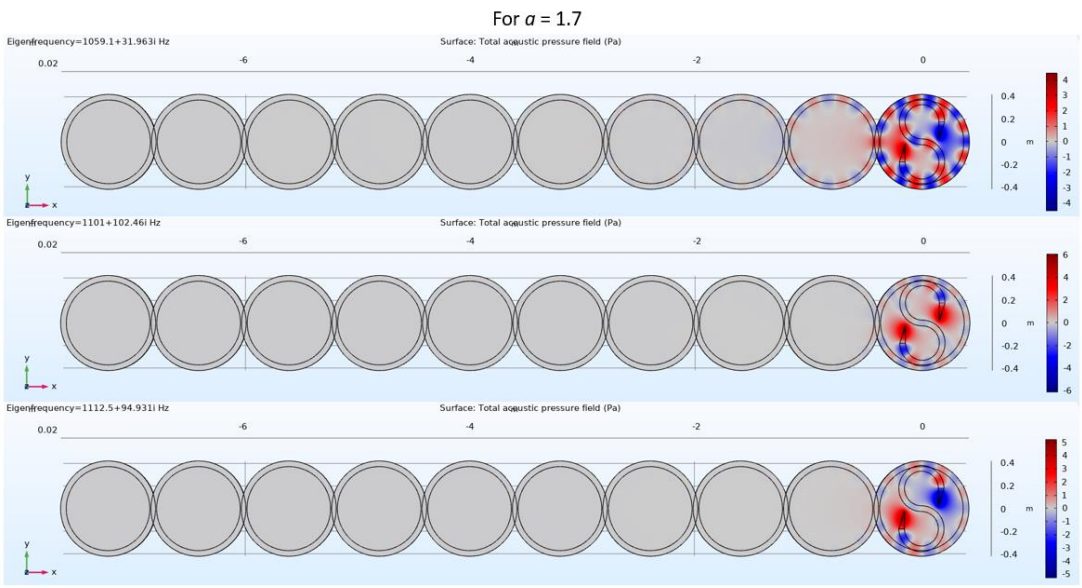

Fig.5.6 Schematic of the pressure fields for a system with loss parameter $a = 1.7$. The figure shows strong localization of fields in the frequencies $1059.1 + 31.96i\ Hz, 1101 + 102.46i\ Hz$, and $1112.5 + 94.931i\ Hz$ when $a = 1.7$.

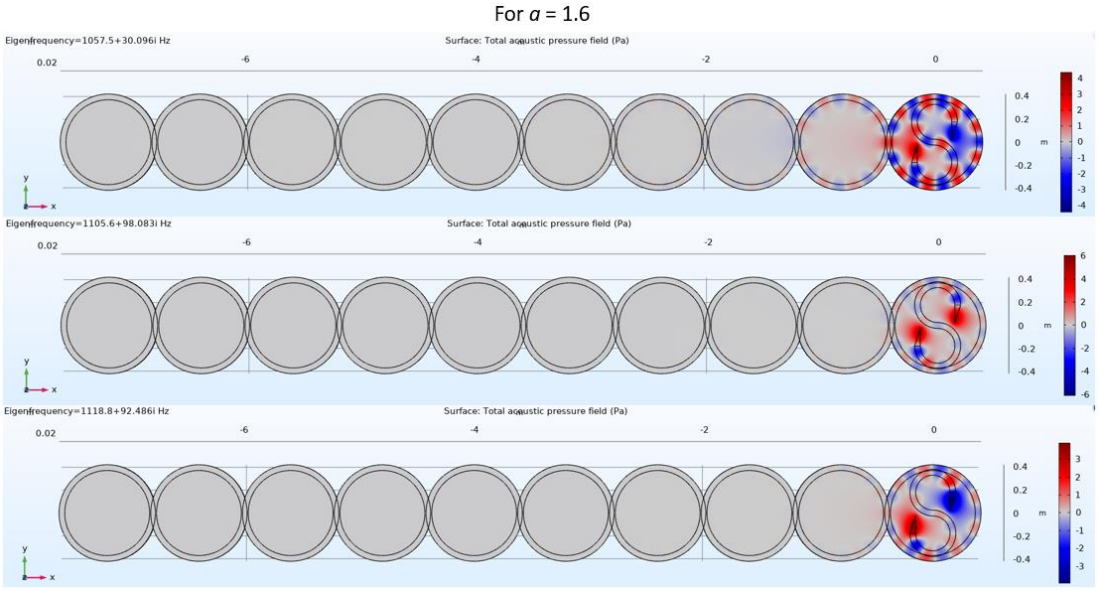

Fig.5.7 Schematic of the pressure fields for a system with loss parameter $a = 1.6$. The figure shows strong localization of fields in the frequencies $1057.5 + 30.096i\ Hz, 1105.6 + 98.083i\ Hz$, and $1118.8 + 92.486i\ Hz$ when $a = 1.6$.

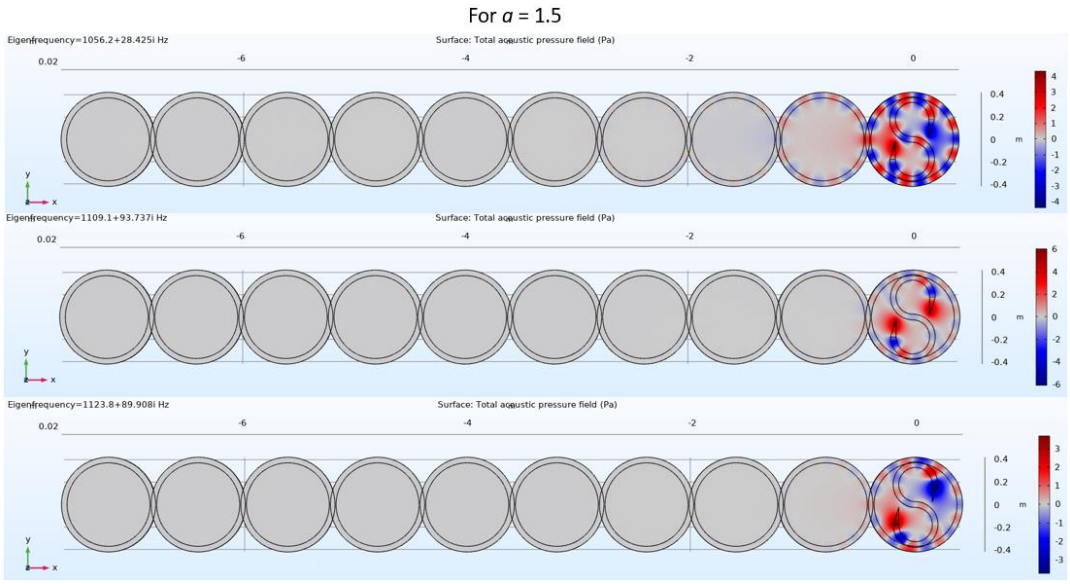

Fig.5.8 Schematic of the pressure fields for a system with loss parameter $a = 1.5$. The figure shows strong localization of fields in the frequencies $1056.2 + 28.425i\ Hz, 1109.1 + 93.737i\ Hz$, and $1123.8 + 89.908i\ Hz$ when $a = 1.5$.

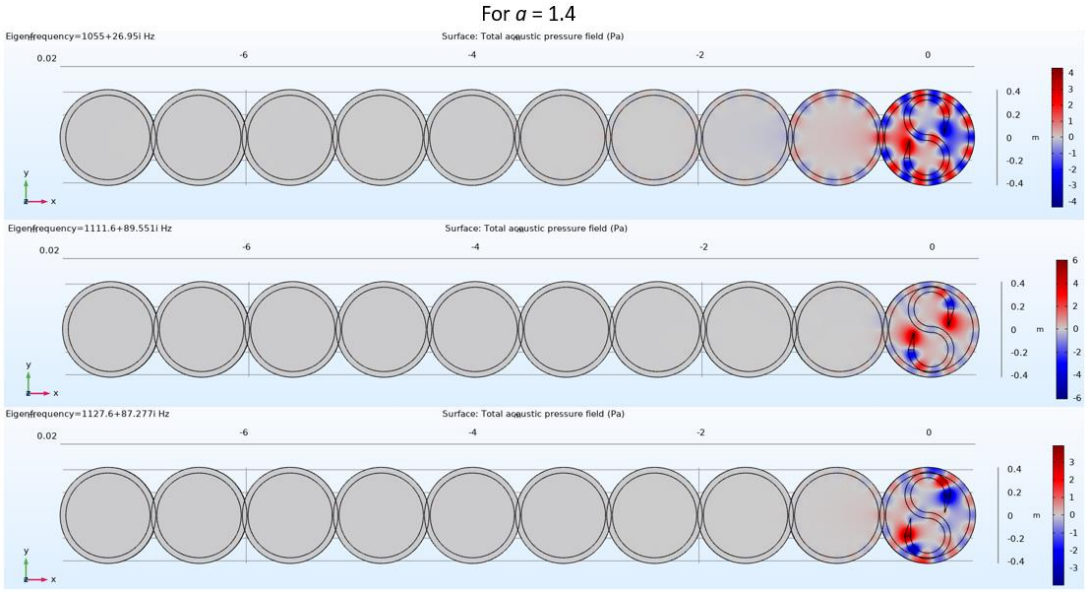

Fig.5.9 Schematic of the pressure fields for a system with loss parameter $a = 1.4$. The figure shows strong localization of fields in the frequencies $1055 + 26.95i\ Hz, 1111.6 + 89.551i\ Hz$, and $1127.6 + 87.227i\ Hz$ when $a = 1.4$.

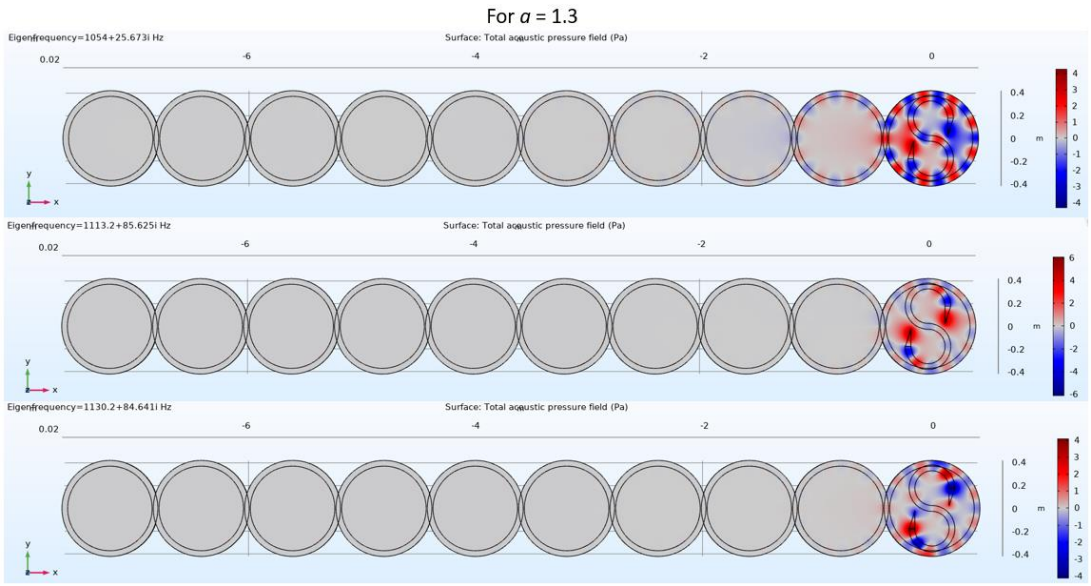

Fig.5.10 Schematic of the pressure fields for a system with loss parameter $a = 1.3$. The figure shows strong localization of fields in the frequencies $1054 + 25.673i\ Hz, 1113.2 + 85.625i\ Hz$, and $1130.2 + 84.641i\ Hz$ when $a = 1.3$.

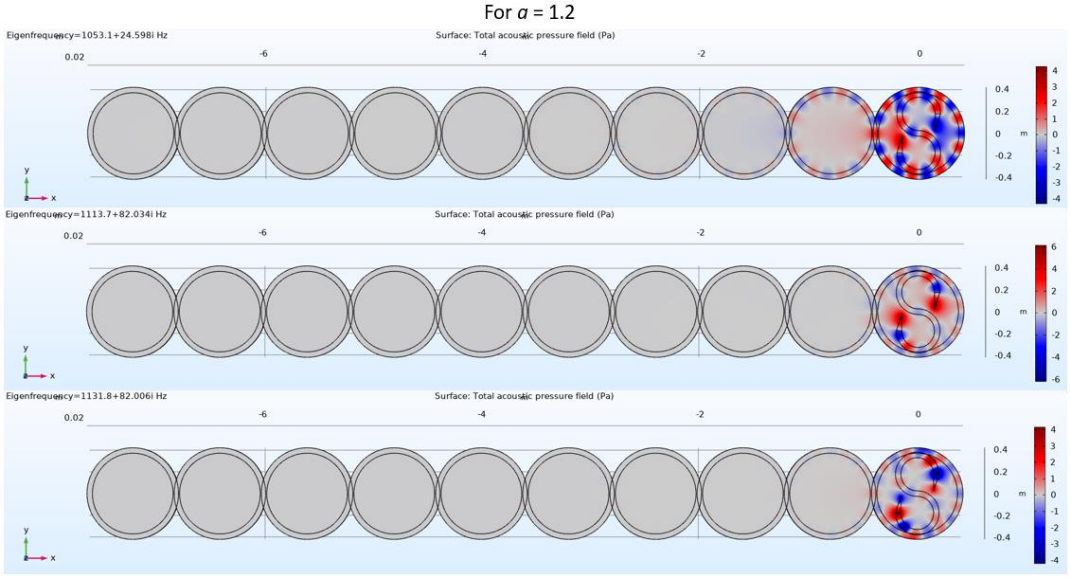

Fig.5.11 Schematic of the pressure fields for a system with loss parameter $a = 1.2$. The figure shows strong localization of fields in the frequencies $1053.1 + 24.598i\ Hz, 1113.7 + 82.034i\ Hz$, and $1131.8 + 82.006i\ Hz$ when $a = 1.2$.

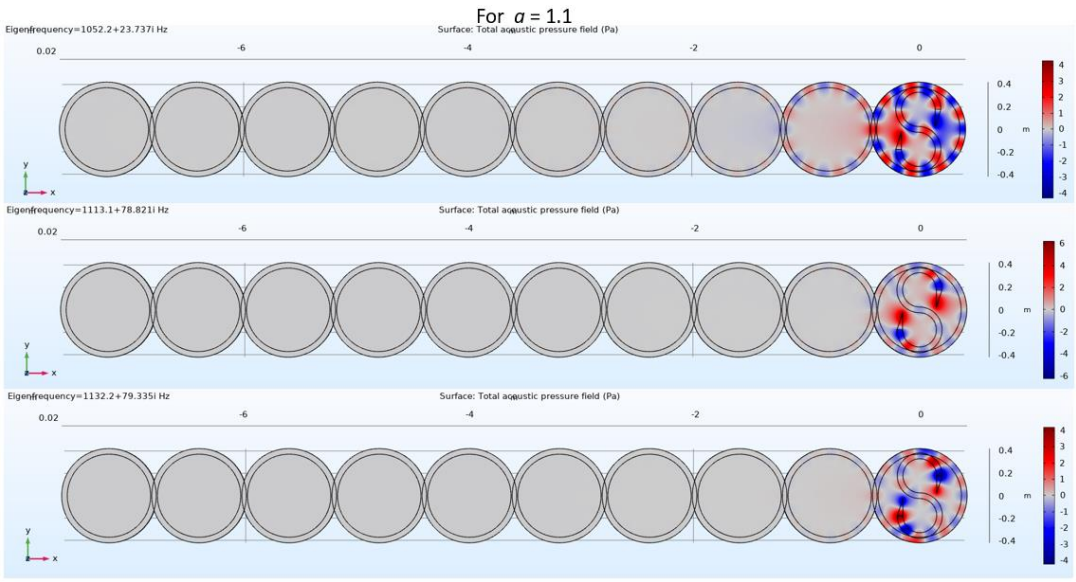

Fig.5.12 Schematic of the pressure fields for a system with loss parameter $a = 1.1$. The figure shows strong localization of fields in the frequencies $1052.2 + 23.737i\ Hz, 1113.1 + 78.821i\ Hz$, and $1132.2 + 79.335i\ Hz$ when $a = 1.1$.

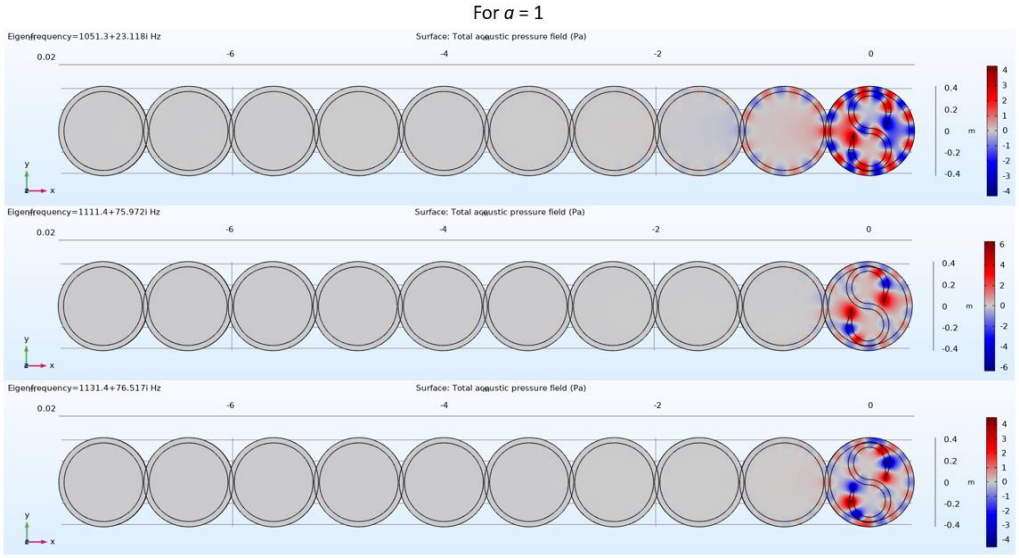

Fig.5.13 Schematic of the pressure fields for a system with loss parameter $a = 1.0$. The figure shows strong localization of fields in the frequencies $1051.3 + 23.118i\ Hz, 1111.4 + 75.972i\ Hz$, and $1131.4 + 76.517i\ Hz$ when $a = 1.0$.

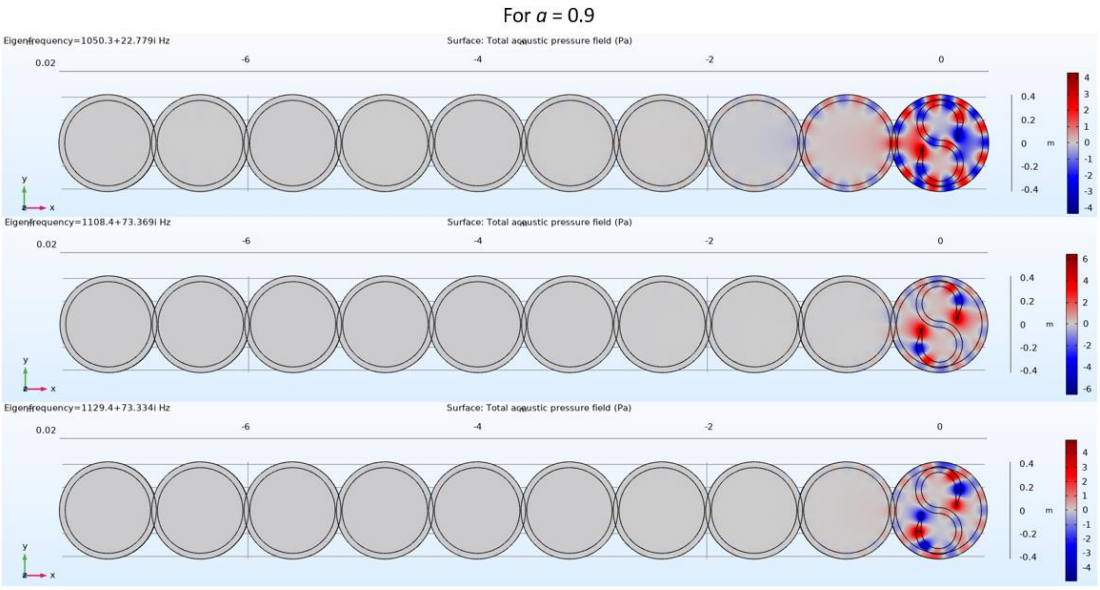

Fig.5.14 Schematic of the pressure fields for a system with loss parameter $a = 0.9$. The figure shows strong localization of fields in the frequencies $1050.3 + 22.779i\ Hz$, $1108.4 + 73.369i\ Hz$, and $1129.4 + 73.334i\ Hz$ when $a = 0.9$.

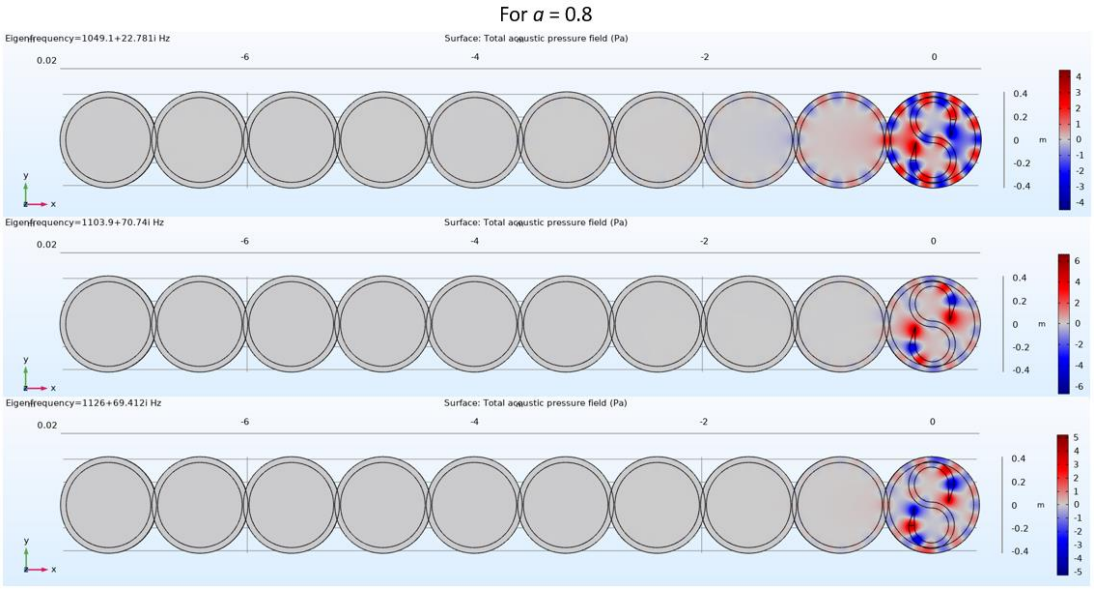

Fig.5.15 Schematic of the pressure fields for a system with loss parameter $a = 0.8$. The figure shows strong localization of fields in the frequencies $1049.1 + 22.781i\ Hz$, $1103.9 + 70.74i\ Hz$, and $1126 + 69.412i\ Hz$ when $a = 0.8$.

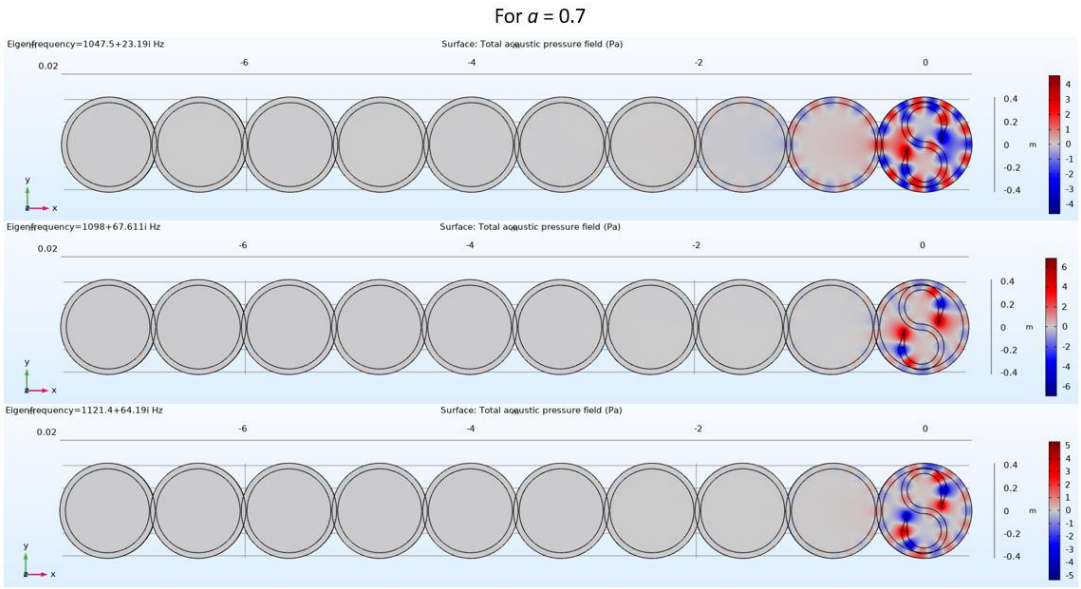

Fig.5.16 Schematic of the pressure fields for a system with loss parameter $a = 0.7$. The figure shows strong localization of fields in the frequencies $1047.5 + 23.19i\ Hz, 1098 + 67.61i\ Hz$, and $1121.4 + 64.19i\ Hz$ when $a = 0.7$.

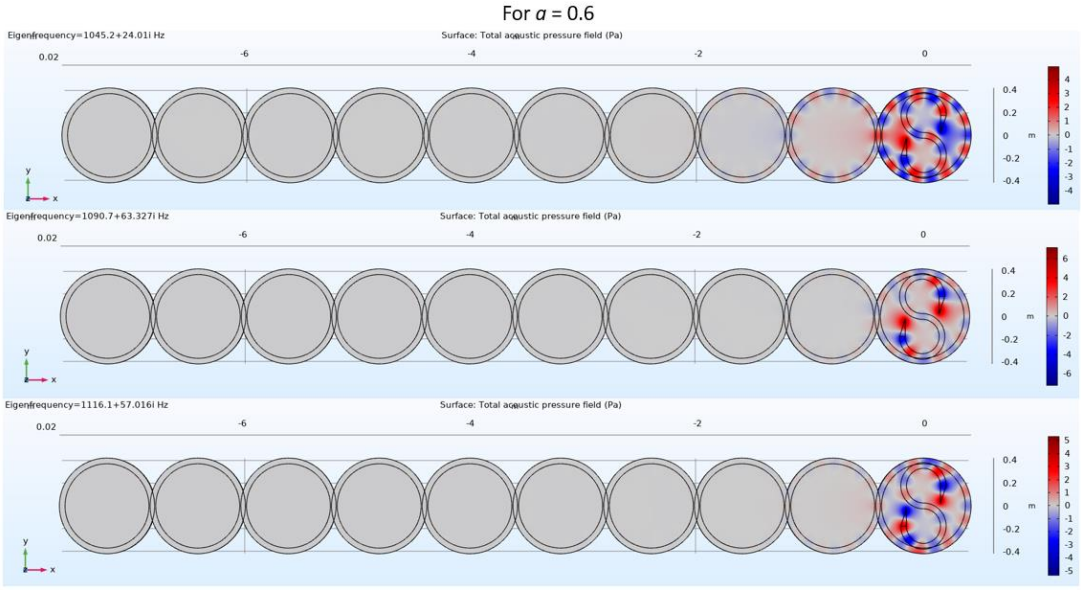

Fig.5.17 Schematic of the pressure fields for a system with loss parameter $a = 0.6$. The figure shows strong localization of fields in the frequencies $1045.2 + 24.01i\ Hz, 1090.7 + 63.327i\ Hz$, and $1116.1 + 57.016i\ Hz$ when $a = 0.6$.

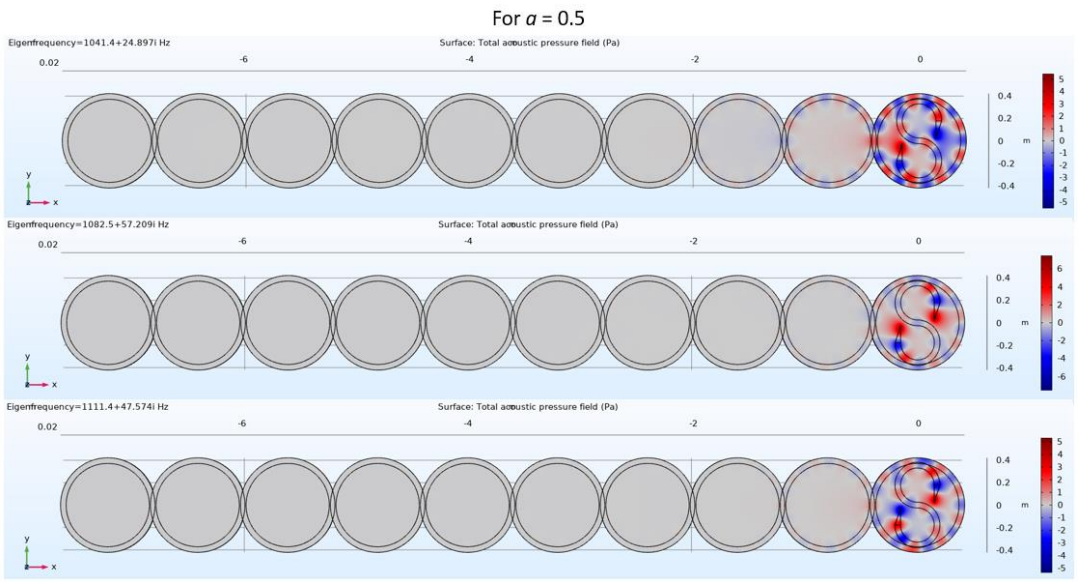

Fig.5.18 Schematic of the pressure fields for a system with loss parameter $a = 0.5$. The figure shows strong localization of fields in the frequencies $1041.4 + 24.897i\ Hz, 1082.5 + 57.209i\ Hz$, and $1111.4 + 47.574i\ Hz$ when $a = 0.5$.

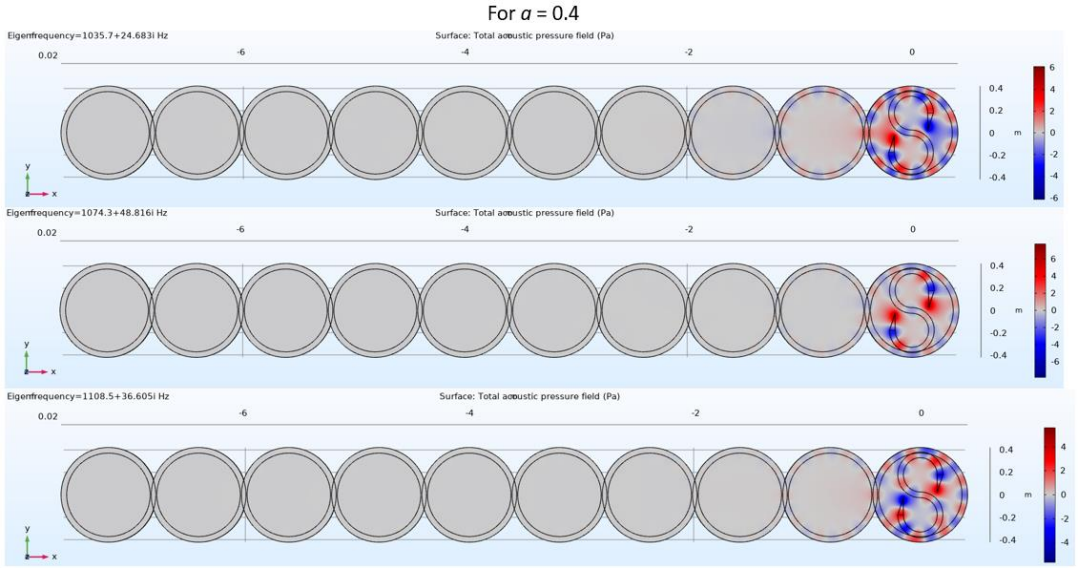

Fig.5.19 Schematic of the pressure fields for a system with loss parameter $a = 0.4$. The figure shows strong localization of fields in the frequencies $1035.7 + 24.683i\ Hz, 1074.3 + 48.816i\ Hz$, and $1108.5 + 36.605i\ Hz$ when $a = 0.4$.

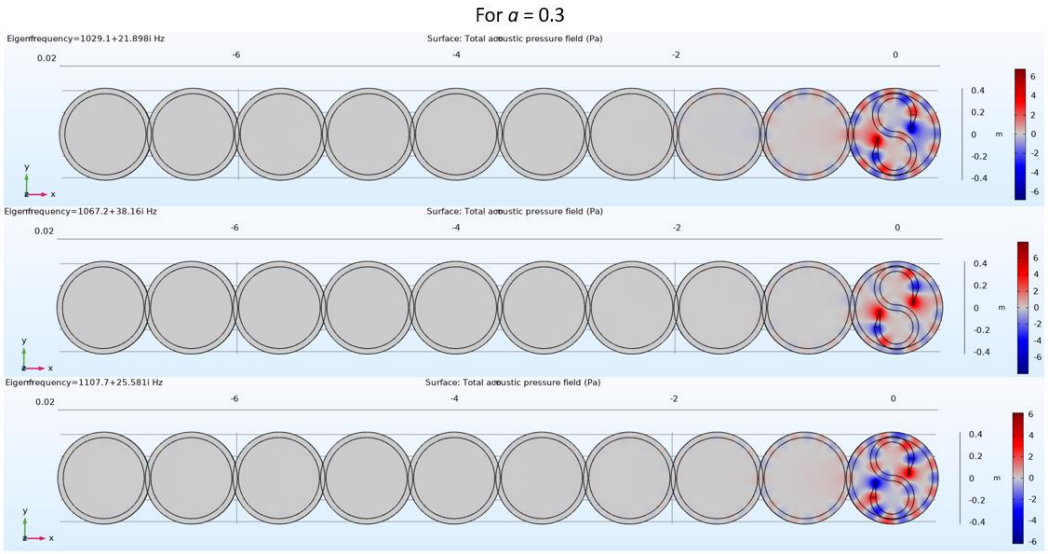

Fig.5.20 Schematic of the pressure fields for a system with loss parameter $a = 0.3$. The figure shows strong localization of fields in the frequencies $1029.1 + 21.898i\ Hz, 1067.2 + 38.16i\ Hz$, and $1107.7 + 25.58i\ Hz$ when $a = 0.3$.

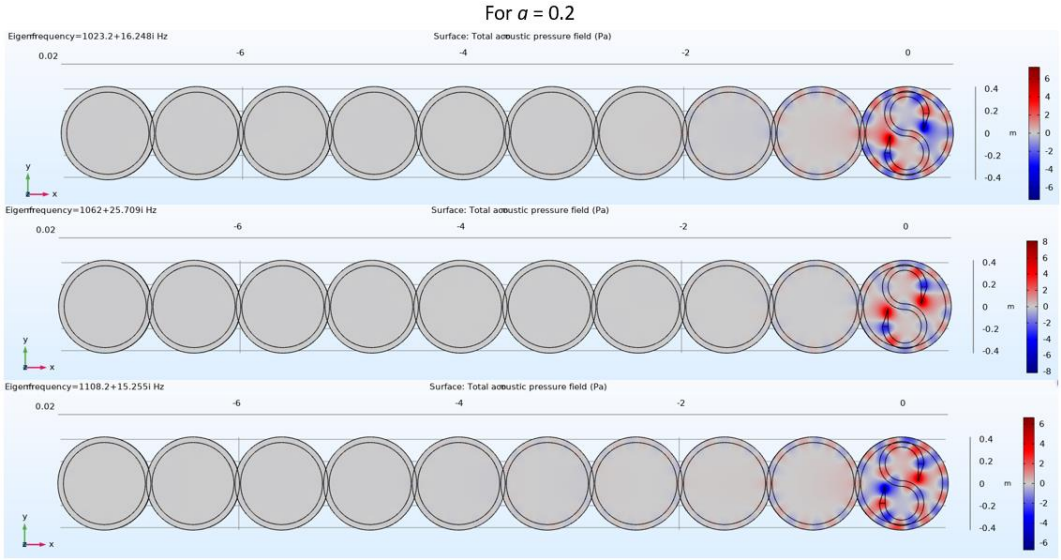

Fig.5.21 Schematic of the pressure fields for a system with loss parameter $a = 0.2$. The figure shows strong localization of fields in the frequencies $1023.2 + 16.248i\ Hz, 1062 + 25.709i\ Hz$, and $1108.2 + 15.255i\ Hz$ when $a = 0.2$.

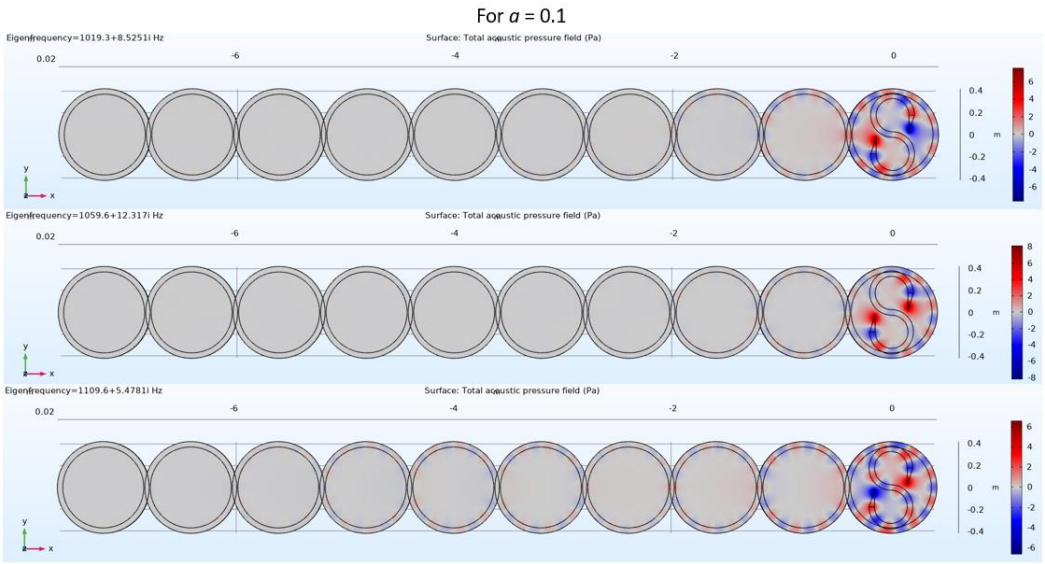

Fig.5.22 Schematic of the pressure fields for a system with loss parameter $a = 0.1$. The figure shows strong localization of fields in the frequencies $1019.3 + 8.525i\ Hz, 1059.6 + 12.317i\ Hz$, and $1109.6 + 5.4781i\ Hz$ when $a = 0.1$.

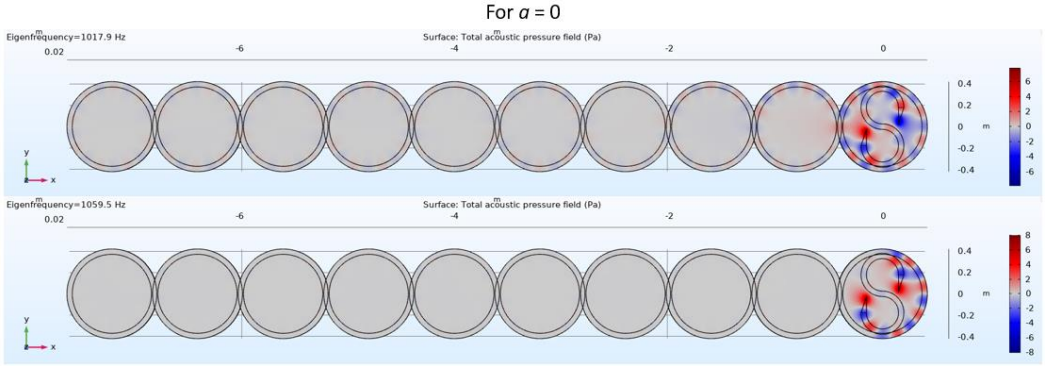

Fig.5.23 Schematic of the pressure fields for a system with loss parameter $a = 0$. The figure shows strong localization of fields in the frequencies $1017.9Hz$, and $1059.5\ Hz$ when $a = 0$.

Table 5.1 Field localization observed for the loss parameter value $a = 2.0\ to\ a = 0$ in decreasing order.

Loss parameter a	*Localization frequency (Hz)*		
	1st	*2nd*	*3rd*
2.0	*1067.2 + 38.04i*	*1079.7 + 113.67i*	*1082.4 + 100.25i*
1.9	*1063.7 + 36.12i*	*1088.2 + 110.58i*	*1094.7 + 98.93i*
1.8	*1061.1 +34.004i*	*1095.2 + 106.72i*	*1104.6 +97.127i*
1.7	*1059.1 +31.96i*	*1101 + 102.46i*	*1112.5 + 94.93i*
1.6	*1057.5 + 30.096i*	*1105.6 + 98.083i*	*1118.8 + 92.48i*
1.5	*1056.2 +28.42i*	*1109.1 + 93.73i*	*1123.8 + 89.9.8i*
1.4	*1055 + 26.95i*	*1111.6 + 89.55i*	*1127.6 +87.27i*
1.3	*1054 +25.67i*	*111.2 + 85.625i*	*1130.2 + 84.64i*
1.2	*1053.1 24.59i*	*1113.7+82.03i*	*1131.8 + 82.006i*
1.1	*1052.2 +23.73i*	*1113.1 + 78.821i*	*1132.2 + 79.335i*
1.0	*1051.3 +23.118i*	*1111.4 + 75.97i*	*1131.4 + 76.517i*
0.9	*1050 +22.77i*	*1108.4 + 73.36i*	*1129.4 + 73.33i*
0.8	*1049.1 + 22.78i*	*1103.9 + 70.74i*	*1126 + 69.412i*
0.7	*1047.5 + 23.19i*	*1098 + 67.61i*	*1121.4 + 64.19i*
0.6	*1045.2 + 24.01i*	*1090.7 + 63.327i*	*1116.1 + 57.016i*
0.5	*1041.4 + 24.89i*	*1082.5 + 57.209i*	*1111.4 + 47.57i*
0.4	*1035.7 24.68i*	*1074.3 + 48.816i*	*1108.5 + 36.6.5i*
0.3	*1029.1 +21.898i*	*1067.2 + 38.16i*	*1107.7 + 25.58i*
0.2	*1023.2 + 16.248i*	*1062 + 25.709i*	*1108.2 + 15.255i*
0.1	*1019.3 + 8.525i*	*1059.6 + 12.317i*	*1109.6 +5.478i*
0	*1017.9*	*1059.5*	-

5.5 Summary and Future Prospects

In conclusion, we studied the geometry-induced non-Hermitian mode couplings and study the different modes in a system of non-Hermitian acoustic ring resonators in whispering gallery mode and the pressure field localization within the system. We have shown that by the introduction of non-Hermiticity in the system of coupled acoustic ring resonators we were able to tune the field localization that occurs in the various eigenfrequencies. It was also observed that we can generate a field localization with the introduction of non-Hermiticity in the system. By changing the degree of non-Hermiticity we can selectively generate the field localization in certain frequencies. Moreover, our proposed design can have application in designing compact isolators, circulators, unidirectional sensors, and filters.

CHAPTER VI

CONCLUSION

In this thesis, we explored the concept of phononic crystal and designed a tunable acoustic filter utilizing the induced non-Hermiticity in the system. We studied the concept of the band structure of a phononic crystal and the occurrence of complete bandgaps in its band structure. Exploring the effect of non-Hermiticity in the phononic crystal we applied the concept to our proposed model and studied its influence in the field propagation within the phononic crystal. The non-Hermiticity is induced as losses in a phononic lattice. The value of which can be changed in order to alter the degree of non-Hermiticity. Based on this we can filter/eliminate specific frequencies from an upcoming signal at will.

We designed our proposed tunable filter that is made of a phononic super-lattice formed by the superposition of two sublattices. We chose the geometry of the two sublattices in a way such that their bandstructure differs from each other. Besides, we introduced non-Hermiticity in one of the sublattices by introducing the complex bulk modulus in the material (air in our case) that the lattice is composed of. The resulting model works as a filter depending on the degree of non-Hermiticity introduced. The larger the degree of non-Hermiticity, the more the generation of absorbed resonances that appear in the reflected spectrum. This provided us a powerful knob to absorb or reflect several frequencies at will with high accuracy. The number of filtered frequencies can be controlled by designing the resonances in the first sublattice. By exploiting this we were able to eliminate the specific frequencies at will.

Using commercial computational software, we design our proposed tunable filter made of a phononic super-lattice. We discussed the steps taken to simulate our model using the COMSOL Multiphysics software, beginning with setting up the model environment followed by building geometry and specifying the materials and material properties. Then we defined the physics for the model and the appropriate boundary conditions for the simulation.

In conclusion, we have proposed and designed a tunable phononic filter based on the superposition of two sub-lattices, one passive and the other with tunable loss. The filtering process in our proposed structure occurs in the reflected field. Apart from the tunability or filter is working based on the resonances and thus can accurately filter specific frequencies. Thus by designing the resonances in the Hermitian lattice and increasing the loss one can remove specific frequencies on the reflected wave at will. Our proposed tunable filter can be easily adapted to the microwave domain as well as photonic structures.

We also studied the geometry-induced non-Hermitian mode couplings and studied different modes in a system of non-Hermitian acoustic ring resonators. We have shown by introducing the non-Hermiticity in the system of coupled acoustic ring resonators we can tune the field localization that occurs in the various eigenfrequencies. By changing the degree of non-Hermiticity we can selectively generate the field localization in certain frequencies. Moreover, our proposed design can have application in designing compact isolators, circulators, unidirectional sensors, and filters.

REFERENCES

Allein, F., Tournat, V., Gusev, V. E., & Theocharis, G. (2016). Tunable magneto-granular phononic crystals. *Applied Physics Letters*, *108*(16), 161903. https://doi.org/10.1063/1.4947192

Aly, A. H., & Mehaney, A. (2012). Enhancement of phononic band gaps in ternary/binary structure. *Physica B: Condensed Matter*, *407*(21), 4262–4268. https://doi.org/10.1016/j.physb.2012.07.014

Andreassen, E., & Jensen, J. S. (2013). Analysis of Phononic Bandgap Structures With Dissipation. *Journal of Vibration and Acoustics*, *135*(4), 041015. https://doi.org/10.1115/1.4023901

Aurégan, Y., & Pagneux, V. (2017). P T -Symmetric Scattering in Flow Duct Acoustics. *Physical Review Letters*, *118*(17), 174301. https://doi.org/10.1103/PhysRevLett.118.174301

Bergamini, A., Delpero, T., Simoni, L. D., Lillo, L. D., Ruzzene, M., & Ermanni, P. (2014). Phononic Crystal with Adaptive Connectivity. *Advanced Materials*, *26*(9), 1343–1347. https://doi.org/10.1002/adma.201305280

Bian, Z., Peng, W., & Song, J. (2014). Thermal Tuning of Band Structures in a One-Dimensional Phononic Crystal. *Journal of Applied Mechanics*, *81*(4), 041008. https://doi.org/10.1115/1.4025058

Bilal, O. R., Foehr, A., & Daraio, C. (2017). Reprogrammable Phononic Metasurfaces. *Advanced Materials*, *29*(39), 1700628. https://doi.org/10.1002/adma.201700628

Bloch, F. (1929). ber die Quantenmechanik der Elektronen in Kristallgittern. *Zeitschrift f r Physik*, *52*(7–8), 555–600. https://doi.org/10.1007/BF01339455

Boechler, N., Theocharis, G., & Daraio, C. (2011). Bifurcation-based acoustic switching and rectification. *Nature Materials*, *10*(9), 665–668. https://doi.org/10.1038/nmat3072

Caleap, M., & Drinkwater, B. W. (2014). Acoustically trapped colloidal crystals that are reconfigurable in real time. *Proceedings of the National Academy of Sciences*, *111*(17), 6226–6230. https://doi.org/10.1073/pnas.1323048111

Camley, R. E., Djafari-Rouhani, B., Dobrzynski, L., & Maradudin, A. A. (1983). Transverse elastic waves in periodically layered infinite and semi-infinite media. *Physical Review B*, *27*(12), 7318–7329. https://doi.org/10.1103/PhysRevB.27.7318

Celli, P., & Gonella, S. (2015). Tunable directivity in metamaterials with reconfigurable cell symmetry. *Applied Physics Letters*, *106*(9), 091905. https://doi.org/10.1063/1.4914011

Chen, A., Wang, Y., Yu, G., Guo, Y., & Wang, Z. (2008). Elastic wave localization in two-dimensional phononic crystals with one-dimensional quasi-periodicity and random disorder. *Acta Mechanica Solida Sinica*, *21*(6), 517–528. https://doi.org/10.1007/s10338-008-0862-x

Christensen, J., Willatzen, M., Velasco, V. R., & Lu, M.-H. (2016). Parity-Time Synthetic Phononic Media. *Physical Review Letters*, *116*(20), 207601. https://doi.org/10.1103/PhysRevLett.116.207601

Cummer, S. A., & Schurig, D. (2007). One path to acoustic cloaking. *New Journal of Physics*, *9*(3), 45–45. https://doi.org/10.1088/1367-2630/9/3/045

Deymier, P. A. (Ed.). (2013). *Acoustic Metamaterials and Phononic Crystals* (Vol. 173). Springer Berlin Heidelberg. https://doi.org/10.1007/978-3-642-31232-8

Ding, K., Zhang, Z. Q., & Chan, C. T. (2015). Coalescence of exceptional points and phase diagrams for one-dimensional P T -symmetric photonic crystals. *Physical Review B*, *92*(23), 235310. https://doi.org/10.1103/PhysRevB.92.235310

Farnell, G. W. (1988). Acoustic Properties of Periodic Layers. In D. F. Parker & G. A. Maugin (Eds.), *Recent Developments in Surface Acoustic Waves* (Vol. 7, pp. 218–235). Springer Berlin Heidelberg. https://doi.org/10.1007/978-3-642-83508-7_23

Feng, L., El-Ganainy, R., & Ge, L. (2017). Non-Hermitian photonics based on parity–time symmetry. *Nature Photonics*, *11*(12), 752–762. https://doi.org/10.1038/s41566-017-0031-1

Fleury, R., Sounas, D., & Alù, A. (2015). An invisible acoustic sensor based on parity-time symmetry. *Nature Communications*, *6*(1), 5905. https://doi.org/10.1038/ncomms6905

Givoli, D., & Neta, B. (2003). High-order non-reflecting boundary scheme for time-dependent waves. *Journal of Computational Physics*, *186*(1), 24–46. https://doi.org/10.1016/S0021-9991(03)00005-6

Grimsditch, M. (1985). Effective elastic constants of superlattices. *Physical Review B*, *31*(10), 6818–6819. https://doi.org/10.1103/PhysRevB.31.6818

Hou, Z., & Assouar, B. M. (2015). Tunable solid acoustic metamaterial with negative elastic modulus. *Applied Physics Letters*, *106*(25), 251901. https://doi.org/10.1063/1.4922873

Jensen, J. S. (2003). Phononic band gaps and vibrations in one- and two-dimensional mass–spring structures. *Journal of Sound and Vibration*, *266*(5), 1053–1078. https://doi.org/10.1016/S0022-460X(02)01629-2

Joannopoulos, J. D. (Ed.). (2008). *Photonic crystals: Molding the flow of light* (2nd ed). Princeton University Press.

Khelif, A., & Adibi, A. (Eds.). (2016). *Phononic crystals: Fundamentals and applications*. Springer. https://doi.org/10.1007/9781461493938

Kushwaha, M. S., Halevi, P., Dobrzynski, L., & Djafari-Rouhani, B. (1993). Acoustic band structure of periodic elastic composites. *Physical Review Letters*, *71*(13), 2022–2025. https://doi.org/10.1103/PhysRevLett.71.2022

Kushwaha, M. S., Halevi, P., Martínez, G., Dobrzynski, L., & Djafari-Rouhani, B. (1994). Theory of acoustic band structure of periodic elastic composites. *Physical Review B*, *49*(4), 2313–2322. https://doi.org/10.1103/PhysRevB.49.2313

Kushwaha, Manvir S. (1997). Stop-bands for periodic metallic rods: Sculptures that can filter the noise. *Applied Physics Letters*, *70*(24), 3218–3220. https://doi.org/10.1063/1.119130

Landau, L. D., Kosevich, A. M., Lifshitz E. M, & Pitaevskiĭ, L. P. (1986). *Theory of elasticity*. https://www.sciencedirect.com/book/9780080570693/theory-of-elasticity

Langley, R. S. (1994). On The Forced Response Of One-dimensional Periodic Structures: Vibration Localization By Damping. *Journal of Sound and Vibration*, *178*(3), 411–428. https://doi.org/10.1006/jsvi.1994.1495

Larabi, H., Pennec, Y., Djafari-Rouhani, B., & Vasseur, J. O. (2007). Multicoaxial cylindrical inclusions in locally resonant phononic crystals. *Physical Review E*, *75*(6), 066601. https://doi.org/10.1103/PhysRevE.75.066601

Li, F., Anzel, P., Yang, J., Kevrekidis, P. G., & Daraio, C. (2014). Granular acoustic switches and logic elements. *Nature Communications*, *5*(1), 5311. https://doi.org/10.1038/ncomms6311

Li, Y., Shen, C., Xie, Y., Li, J., Wang, W., Cummer, S. A., & Jing, Y. (2017). Tunable Asymmetric Transmission via Lossy Acoustic Metasurfaces. *Physical Review Letters*, *119*(3), 035501. https://doi.org/10.1103/PhysRevLett.119.035501

Liang, B., Guo, X. S., Tu, J., Zhang, D., & Cheng, J. C. (2010). An acoustic rectifier. *Nature Materials*, *9*(12), 989–992. https://doi.org/10.1038/nmat2881

Liu, Z. (2000). Locally Resonant Sonic Materials. *Science*, *289*(5485), 1734–1736. https://doi.org/10.1126/science.289.5485.1734

Molerón, M., Serra-Garcia, M., & Daraio, C. (2016). Visco-thermal effects in acoustic metamaterials: From total transmission to total reflection and high absorption. *New Journal of Physics*, *18*(3), 033003. https://doi.org/10.1088/1367-2630/18/3/033003

Montero de Espinosa, F. R., Jiménez, E., & Torres, M. (1998). Ultrasonic Band Gap in a Periodic Two-Dimensional Composite. *Physical Review Letters*, *80*(6), 1208–1211. https://doi.org/10.1103/PhysRevLett.80.1208

Morse, P. M., & Ingard, K. U. (1986). *Theoretical acoustics*. Princeton University Press.

Multiphysics, C. (1998). Introduction to COMSOL multiphysics extregistered. COMSOL Multiphysics, Burlington, MA, Accessed Feb, 9, 2018. (n.d.).

Nemat-Nasser, S., Willis, J. R., Srivastava, A., & Amirkhizi, A. V. (2011). Homogenization of periodic elastic composites and locally resonant sonic materials. *Physical Review B*, *83*(10), 104103. https://doi.org/10.1103/PhysRevB.83.104103

Olsson III, R. H., & El-Kady, I. (2009). Microfabricated phononic crystal devices and applications. *Measurement Science and Technology*, *20*(1), 012002. https://doi.org/10.1088/0957-0233/20/1/012002

Pennec, Y., Vasseur, J. O., Djafari-Rouhani, B., Dobrzyński, L., & Deymier, P. A. (2010). Two-dimensional phononic crystals: Examples and applications. *Surface Science Reports*, *65*(8), 229–291. https://doi.org/10.1016/j.surfrep.2010.08.002

Poshakinskiy, A. V., Poddubny, A. N., & Fainstein, A. (2016). Multiple Quantum Wells for P T -Symmetric Phononic Crystals. *Physical Review Letters*, *117*(22), 224302. https://doi.org/10.1103/PhysRevLett.117.224302

Ramezani, H., Dubois, M., Wang, Y., Shen, Y. R., & Zhang, X. (2016). Directional excitation without breaking reciprocity. *New Journal of Physics*, *18*(9), 095001. https://doi.org/10.1088/1367-2630/18/9/095001

Robillard, J.-F., Matar, O. B., Vasseur, J. O., Deymier, P. A., Stippinger, M., Hladky-Hennion, A.-C., Pennec, Y., & Djafari-Rouhani, B. (2009). Tunable magnetoelastic phononic crystals. *Applied Physics Letters*, *95*(12), 124104. https://doi.org/10.1063/1.3236537

Sánchez-Pérez, J. V., Caballero, D., Mártinez-Sala, R., Rubio, C., Sánchez-Dehesa, J., Meseguer, F., Llinares, J., & Gálvez, F. (1998). Sound Attenuation by a Two-Dimensional Array of Rigid Cylinders. *Physical Review Letters*, *80*(24), 5325–5328. https://doi.org/10.1103/PhysRevLett.80.5325

Shi, C., Dubois, M., Chen, Y., Cheng, L., Ramezani, H., Wang, Y., & Zhang, X. (2016). Accessing the exceptional points of parity-time symmetric acoustics. *Nature Communications*, *7*(1), 11110. https://doi.org/10.1038/ncomms11110

Sigalas, M., & Economou, E. N. (1993). Band structure of elastic waves in two dimensional systems. *Solid State Communications*, *86*(3), 141–143. https://doi.org/10.1016/0038-1098(93)90888-T

Sigalas, M. M., & Economou, E. N. (1992). Elastic and acoustic wave band structure. *Journal of Sound and Vibration*, *158*(2), 377–382. https://doi.org/10.1016/0022-460X(92)90059-7

Sigalas, Mihail, Kushwaha, M. S., Economou, E. N., Kafesaki, M., Psarobas, I. E., & Steurer, W. (2005). Classical vibrational modes in phononic lattices: Theory and experiment. *Zeitschrift Für Kristallographie - Crystalline Materials*, *220*(9–10). https://doi.org/10.1524/zkri.2005.220.9-10.765

Vasseur, J. O., Deymier, P. A., Chenni, B., Djafari-Rouhani, B., Dobrzynski, L., & Prevost, D. (2001). Experimental and Theoretical Evidence for the Existence of Absolute Acoustic Band Gaps in Two-Dimensional Solid Phononic Crystals. *Physical Review Letters*, *86*(14), 3012–3015. https://doi.org/10.1103/PhysRevLett.86.3012

Vasseur, J. O., Deymier, P. A., Frantziskonis, G., Hong, G., Djafari-Rouhani, B., & Dobrzynski, L. (1998). Experimental evidence for the existence of absolute acoustic band gaps in two-dimensional periodic composite media. *Journal of Physics: Condensed Matter*, *10*(27), 6051–6064. https://doi.org/10.1088/0953-8984/10/27/006

Vasseur, J. O., Matar, O. B., Robillard, J. F., Hladky-Hennion, A.-C., & Deymier, P. A. (2011). Band structures tunability of bulk 2D phononic crystals made of magneto-elastic materials. *AIP Advances*, *1*(4), 041904. https://doi.org/10.1063/1.3676172

Wang, P., Casadei, F., Shan, S., Weaver, J. C., & Bertoldi, K. (2014). Harnessing Buckling to Design Tunable Locally Resonant Acoustic Metamaterials. *Physical Review Letters*, *113*(1), 014301. https://doi.org/10.1103/PhysRevLett.113.014301

Wang, Z., Zhang, Q., Zhang, K., & Hu, G. (2016). Tunable Digital Metamaterial for Broadband Vibration Isolation at Low Frequency. *Advanced Materials*, *28*(44), 9857–9861. https://doi.org/10.1002/adma.201604009

Ward, G. P., Lovelock, R. K., Murray, A. R. J., Hibbins, A. P., Sambles, J. R., & Smith, J. D. (2015). Boundary-Layer Effects on Acoustic Transmission Through Narrow Slit Cavities. *Physical Review Letters*, *115*(4), 044302. https://doi.org/10.1103/PhysRevLett.115.044302

Xiao, Y., Wen, J., Yu, D., & Wen, X. (2013). Flexural wave propagation in beams with periodically attached vibration absorbers: Band-gap behavior and band formation mechanisms. *Journal of Sound and Vibration*, *332*(4), 867–893. https://doi.org/10.1016/j.jsv.2012.09.035

Yablonovitch, E. (1987). Inhibited Spontaneous Emission in Solid-State Physics and Electronics. *Physical Review Letters*, *58*(20), 2059–2062. https://doi.org/10.1103/PhysRevLett.58.2059

Zhang, J., Peng, B., Özdemir, Ş. K., Liu, Y., Jing, H., Lü, X., Liu, Y., Yang, L., & Nori, F. (2015). Giant nonlinearity via breaking parity-time symmetry: A route to low-threshold phonon diodes. *Physical Review B*, *92*(11), 115407. https://doi.org/10.1103/PhysRevB.92.115407

Zhu, X., Ramezani, H., Shi, C., Zhu, J., & Zhang, X. (2014). P T -Symmetric Acoustics. *Physical Review X*, *4*(3), 031042. https://doi.org/10.1103/PhysRevX.4.031042

Zigoneanu, L., Popa, B.-I., Starr, A. F., & Cummer, S. A. (2011). Design and measurements of a broadband two-dimensional acoustic metamaterial with anisotropic effective mass density. *Journal of Applied Physics*, *109*(5), 054906. https://doi.org/10.1063/1.3552990

BIOGRAPHICAL SKETCH

Born on 6th October 1989, in Puranagaun-4, Ramechhap District a remote village of Nepal, Sandeep Puri moved to Kathmandu for his secondary education and later moved to Sikkim, India for his higher education thereafter. He completed his Bachelor of Science and Master of Science in Physics from Sikkim University, Sikkim, India, in 2013 and 2015 respectively. He joined Kurseong College, Darjeeling, India, as a Junior Research Fellow (JRF) from 2018-2019. He obtained his Master of Science in Physics with thesis option from The University of Texas Rio Grande Valley, Texas, USA, in May 2021, where he worked as Graduate Research Assistant and Graduate Teaching Assistant during his first and second year at the UTRGV. His is interest in Material Science, theoretical and Experimental Condensed Matter Physics. His email is sundeepchettri@gmail.com.